To the Graduate Council:

I am submitting herewith a thesis written by Pavlina Jetchkova Jeleva entitled "Cataract Characterization Using Multi-Wavelength Extinction". I have examined the final copy of this thesis for form and content and recommend that it be accepted in partial fulfillment of the requirements for the degree of Master of Science, with a major in Physics.

J. W. L. Lewis, Major Professor

We have read this thesis
and recommend its acceptance:

Christia Parigo

Accepted for the Council:

Interim Vice Provost and
Dean of the Graduate School

Cataract Characterization Using Multi-Wavelength Extinction

A Thesis

Presented for the

Master of Science Degree

The University of Tennessee, Knoxville

Pavlina Jetchkova Jeleva

August 2001

Copyright © Pavlina Jetchkova Jeleva, 2001

All rights reserved

Acknowledgments

I would like to express my appreciation to Dr. J. W. L. Lewis and Dr. C. Parigger for their guidance and support. I would also like to to thank Dr. Chen for her comments about this work. Special "thank you" to I. for being such a good friend and to my family for their patience.

Abstract

The medical condition of cataracts is recognized as major causes of blindness worldwide. Simple, inexpensive screening diagnostic techniques are desired for early detection and quantitative characterization of cataracts. Multiwavelength extinction methods using retinal reflectance are shown to provide this capability. Previous research in the University of Tennessee Space Institute Center for Laser Applications was extended to perform simulated Monte Carlo studies of the technique.

Contents

1 Cataract 1

1.1 Epidemiology of Cataract 1

1.2 The Eye Lens 3

1.3 Factors Causing Cataract 4

1.4 Cataract Classification 7

1.5 Pediatric Cataracts 13

2 Techniques for Cataract Diagnosis 18

2.1 Slit Lamp 18

2.2 Optical Coherence Tomography 20

2.3 Scheimflug Photography 22

3 The Eye Lens 24

3.1 Normal Eye Lens 24

3.2 Eye Lens Proteins 26

3.3 α Crystallin 26

3.4 β Crystallin 28
3.5 Transparency and Transmission of a Normal Eye Lens 29
3.6 Index of Refraction 35
3.7 Aging of the Eye lens 37
3.8 Cataractous Lens 39

4 Particle Size Evaluation **43**
4.1 Introduction 43
4.2 Scattering Techniques 44
4.3 Multi-Wavelength Extinction Measurements 46
4.4 Downhill Simplex Method 48
4.5 Monte Carlo Simulations 49
4.6 Cataract Size Evaluation 49

5 Cataract Size Evaluation Using the Monte Carlo Method **57**
5.1 Simulations 57
5.2 Small particles 58
5.3 Large Particles 68
5.4 Sensitivity Calculations 75
5.5 Benchmark Calculations 78

Bibliography **82**

Vita **94**

List of Tables

1.1 Description of pediatric cataracts [1]. 14

1.2 Average annual number of cataracts (in thousands), by age, race and geographic location. Bold numbers show the rate per thousand [2, 3, 4, 5, 6, 7]. 15

1.3 Average annual number of cataracts (in thousands), by age, race and geographic location. Bold numbers show the rate per thousand [2, 3, 4, 5, 6, 7] 16

List of Figures

1.1 Number of cataract cases versus the total population in the US. 2

1.2 Hypothesis for cataract formation [8]. 5

1.3 Types of cataracts depending on their location. 8

1.4 Lens transparency decrease (up) and lens coloration changes (down) of noncataractous eyes with age [9]. 12

2.1 Diagram of a slitlamp [10]. 19

2.2 Schematic of an optical coherence tomography system [11]. 21

2.3 Illustration of the Scheimflug principle [12]. 21

2.4 Scheimflug slit lamp with a CCD camera [12]. 23

3.1 Layers of the eye lens [10]. 25

3.2 The structure of the alpha-crystallin of humans predicted by Shindyalov and Bourne based on concept of intermediate sequence search[13]. . . . 27

3.3 Structure of bovine $\beta B2$ molecule [14]. 29

3.4 Transmission of the eye lens vs. wavelength [15]. 31

3.5 Optical density of the eye lens as a function of the wavelength. Data taken from [16]. 32

3.6 Optical density of the eye lens as a function of the age. Only the scattering term is taken into account [17]. 33

3.7 The absorption by lens pigment (in percents) as a function of age. ∘, age 21; ×, age 25; △, age 31; •, age45; and +, age 63[17]. 34

3.8 The optical density measured from different authors.∘, Ludvigh and McCarthy [18]; +, Weale (a cloudy portion of a 53-years old lens)[19]; squares, Zigman et al. (cortical cataract); △, Zigman et al. (nuclear and cortical); and ×, Zigman et al. (nuclear and cortical cataract) [17]. 35

3.9 Index of refraction distribution (modified from the original)[20]. 36

3.10 Index of refraction distribution (modified from the original)[20]. 36

3.11 Change of the weight of the eye lens with age [21]. 37

3.12 Change of the size of the eye lens with age [22]. 38

3.13 Dry mass distribution along the lens axis in three normal lenses: A, 62 years old, B, 24 years old and C, 1.5 years old[21]. 38

4.1 Mean diffusivity in a normal human lens as a function of temperature and position in the lenses [23]. 50

4.2 Mean diffusivity in cataractous human lenses as a function of temperature and position. 51

4.3 Size of the protein aggregates as a function of age. 52

4.4 Volume fraction of the protein aggregates as a function of age. 52

4.5 The average distance of separation of protein aggregates as a function of age. 53

4.6 Histogram of the radius of the small proteins [24]. 54

4.7 Histogram of the radius of the large proteins [24]. 54

4.8 Histogram of the radius of the large proteins in a cataractous lens [24]. . 54

4.9 Relative scattering intensity from a rabbit cataract on the axis of the eye lens[25]. 55

5.1 Histogram of the deconvolved particle diameters - 2D deconvolution. Assumed mean diameter 0.5 μm, error level 0.02. 60

5.2 Histogram of the deconvolved variances - 2D deconvolution. Assumed variance 0.05 μm, error level 0.02. 60

5.3 Histogram of the deconvolved particle diameters - 2D deconvolution. Assumed mean diameter 0.5 μm, error level 0.06. 61

5.4 Histogram of the deconvolved variances - 2D deconvolution. Assumed variance 0.05 μm, error level 0.06. 61

5.5 Histogram of the deconvolved particle diameters - 2D deconvolution. Assumed mean diameter 0.5 μm, error level 0.1. 62

5.6 Histogram of the deconvolved variances - 2D deconvolution. Assumed variance 0.05 μm, error level 0.1. 62

5.7 Histogram of the particle diameters - 3D deconvolution. Assumed mean diameter 0.5 μm, error level 0.02. 63

5.8 Histogram of the variances - 3D deconvolution. Assumed variance 0.05 μm, error level 0.02. 63

5.9 Histogram of the NL products - 3D deconvolution. Assumed $NL = 10^9 cm^{-2}$, error level = 0.02. 64

5.10 Histogram of the particle diameters - 3D deconvolution. Assumed mean diameter 0.5 μm, error level 0.06. 64

5.11 Histogram of the variances - 3D deconvolution. Assumed variance 0.05 μm, error level 0.06. 65

5.12 Histogram of the NL products - 3D deconvolution. Assumed $NL = 10^9 cm^{-2}$, error level = 0.06. 65

5.13 Histogram of the particle diameters - 3D deconvolution. Assumed mean diameter 0.5 μm, error level 0.1. 66

5.14 Histogram of the variances - 3D deconvolution. Assumed variance 0.05 μm, error level 0.1. 66

5.15 Histogram of the NL products - 3D deconvolution. Assumed $NL = 10^9 cm^{-2}$, error level = 0.1. 67

5.16 Histogram of the particle diameters - 2D deconvolution. Assumed mean diameter 2.7 μm, error level 0.02. 69

5.17 Histogram of the variances - 2D deconvolution. Assumed variance 0.135 μm, error level 0.02. 69

5.18 Histogram of the particle diameters - 2D deconvolution. Assumed mean diameter 2.7 μm, error level 0.06. 70

5.19 Histogram of the variances - 2D deconvolution. Assumed variance 0.135 μm, error level 0.06. 70

5.20 Histogram of the particle diameters - 2D deconvolution. Assumed mean diameter 2.7 μm, error level 0.1. 71

5.21 Histogram of the variances - 2D deconvolution. Assumed variance 0.135 μm, error level 0.1. 71

5.22 Histogram of the particle diameters - 2D deconvolution. Assumed mean diameter 2.7 μm, error level 0.16. 72

5.23 Histogram of the variances - 2D deconvolution. Assumed variance 0.135 μm, error level 0.16. 72

5.24 Histogram of the diameters - 3D deconvolution. Assumed mean diameter 2.7 μm, error level 0.02. 73

5.25 Histogram of the particle variances - 3D deconvolution. Assumed variance 0.135 μm, error level 0.02. 73

5.26 Histogram of the NL products - 3D deconvolution. Assumed $NL = 10^6 cm^{-2}$, error level = 0.02. 74

5.27 Minimum detectable NL for different particle sizes. 75

5.28 Minimum detectable volume for different particle sizes. 76

5.29 Minimum detectable fraction of the observation volume for different particle sizes. 77

5.30 Benchmark for 2D deconvolution calculations on a single PC. 79

5.31 Benchmark for 2D deconvolution calculations on a single PC. 80

5.32 Benchmark for 2D deconvolution calculations on a Condor loop. 80

5.33 Benchmark for 2D deconvolution calculations on a Condor loop. 81

Chapter 1

Cataract

1.1 Epidemiology of Cataract

The condition of cataracts is the opacity of the eye lens, its capsule or both, which results in the loss of visual acuity and retinal illumination. It has been identified as a major cause of blindness by the World Health Organization (WHO). Specifically, according to the WHO, forty-four percent of the countries included in their Blindness Data Bank report this condition to be the primary cause of blindness. The estimated number of sightless people worldwide is forty-two million, of which seventeen million suffer from cataracts [26].

According to the National Center for Health Statistics (NCHS), the annual number of reported subjects with cataracts in the United States increased from approximately 5.5 million in 1985-87 to seven million in 1996. Taking into account the increase in population shows that the rate of people with cataracts has not increased (see Fig.1.1).

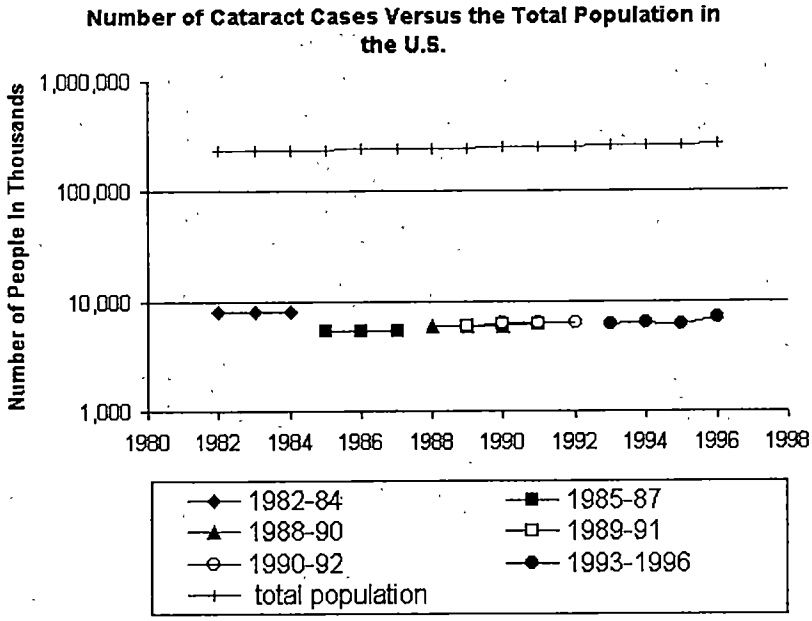


Figure 1.1: Number of cataract cases versus the total population in the US.

Gender, race and geographic region of the U.S. show differences in the frequency of cataracts. Women, non-caucasian, and Southerners exhibit rates of increased incidence of the condition (For more details see Table.1.2).

The only treatment of cataracts so far is replacement of the eye lens with an artificial one. However, there exists the possibility of the development of pharmaceuticals to arrest the growth of cataract once detected. The goal of some research groups, including ours, is to find a method to detect and quantify this disorder in its early stage in order to prevent surgery. Therefore, the early detection of cataract, combined with such drug therapy, can delay the surgical intervention for pediatric and geriatic cataract patients. Such early detection requires the use of inexpensive, rapid screening devices, and the

development of such a technique is an objective of this work.

1.2 The Eye Lens

The eye lens is a transparent, asymmetric, avascular organ, which is seated posterior to the pupil and the iris and anterior to the vitreous. Its anterior-posterior thickness is 4 to 5mm, and is age-dependent. This thickness can also change through the process of accommodation, whose purpose is to focus the image on the retina [27]. The eye lens is embedded in a transparent basement membrane[1], the lens capsule [28]. The thickness of the capsule varies from the posterior to the anterior pole [10]. The epithelial cells produce the anterior capsule, while the posterior part is produced by the fiber cells. The eye lens epithelium is composed of cubic cells, which, after undergoing mitosis, differentiate into lens fiber cells [10, 28]. The lens fibers make up the major part of the eye lens. The newly synthesized fibers push the old ones inwards, and the lens nucleus and cortex are formed. The oldest fibers (present at birth) comprise the nucleus of the lens. It has two zones - embryonic (inner) nucleus and a fetal shell. Later in life the cortex is formed [29].

The transparency and the refractive index gradient of the eye lens is maintained by the unique protein distribution of the eye lens proteins, called crystallins. They constitute more than 90% of the dry mass, and this concentration increases with age. Mechanical or biochemical factors may induce changes in the structure and properties of

[1]basement membrane(basement lamina) is a thin layer of noncellular material of a fine filamentous texture underlying the epithelium [27]

the eye lens fibers and proteins, which can lead to abnormal optical properties of the eye lens tissue. The affected regions of the lens appear opaque or assume different shapes. In all the cases, the light coming to the eye is scattered, and the image on the retina is partially or completely distorted. This state is called a cataract. Microscopically, cataract appears with opened sutures, globule formation, cellular fragmentation and misalignment and protein aggregation.

1.3 Factors Causing Cataract

There does not exist a definite answer to what exactly causes cataract. It may be a factor or a combination of factors. Research has shown that chemical and physiological changes in the lens result from ultraviolet radiation, drugs, age, genetical mutation and other causes. As pointed out by the National Institutes of Health (NIH), these factors can act directly or indirectly (see fig.1.2). Factors may result in changes of the metabolic functions of the eye lens by altering its ion balance, the levels of metabolites, growth factors, oxidants, antioxidants, protein tertiary structure and properties. The major hypothesis explains the age-related cataracts by either a change in the protein-protein interactions leading to protein aggregation or membrane damage. The processes, considered to lead to either change are: oxidative stress, posttranslational modifications of crystallins and the loss of chaperon-like properties of α - crystallin [8].

The UV-B radiation is considered to be one of the major causes of senile cataracts [30]. Only about 11mW/cm^2 of solar radiation above the atmosphere is in the UV

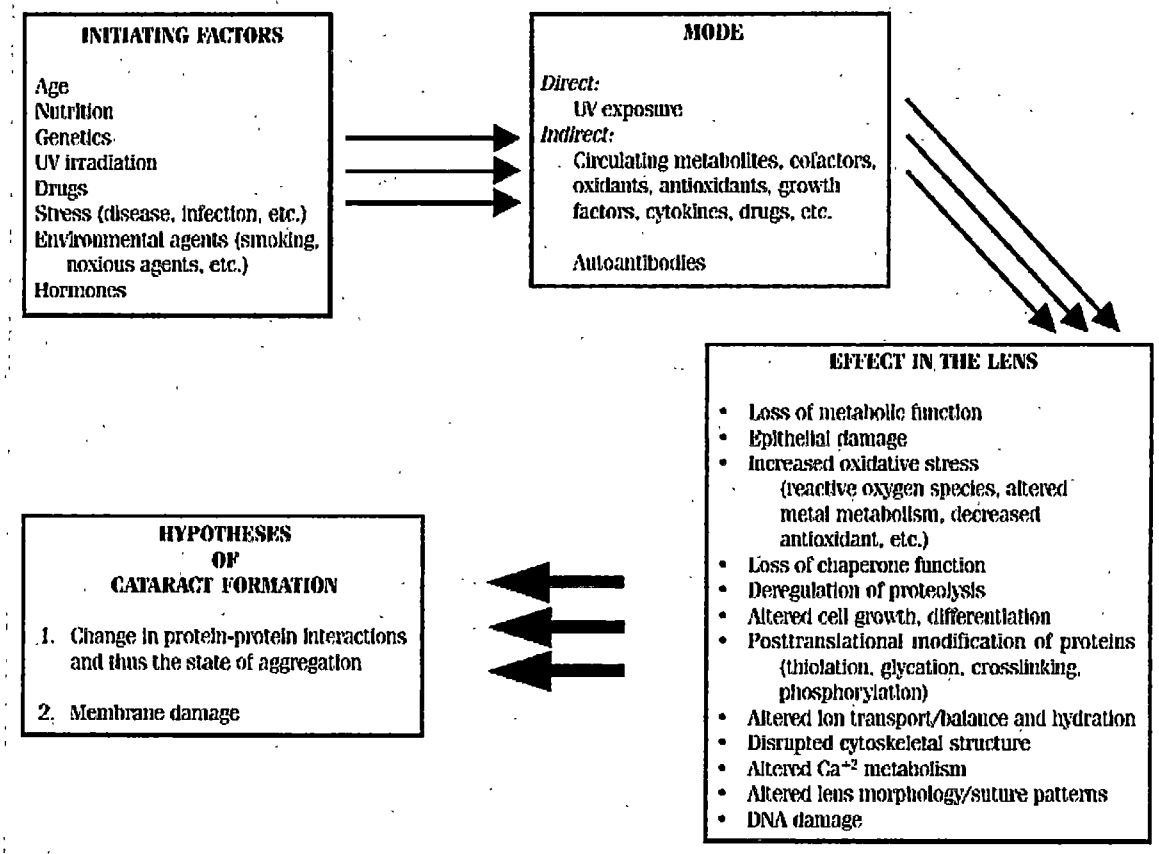


Figure 1.2: Hypothesis for cataract formation [8].

(280-400) nm and of that amount about 2-5mW/cm^2 reach the Earth. The solar flux depends on the geographic location and season [31]. In 1977 Hiller, Giacometti and Yuen [32] performed epidemiological research on the prevalence of cataracts in regions with different amount of sunlight hours. Their results show that there was no greater incidence of cataracts in places with higher sunlight exposure in the age group of (20-44)yrs of age. In contrast, people of age between 65 and 74 in such regions had twice as many cataracts then the others. This ratio becomes even higher for people above the age of 75 years. Another group, led by Zigman showed in 1979 that only the brunescent[1] cataracts are dependent on the geographic region [33].

The mechanisms involved in the formation of the radiation cataracts are initiated by the absorption of the energy of the photons by the molecules in the fiber cells. Some of the resulting processes are: photooxidation of free and protein bound triptophan, DNA damage and disruption of the cation transport [30]. A study by Won Tae Jung [34] shows that the racemidation of aminoacids may cause cataracts by disrupting the protein tertiary structure. He also shows that in a condition of cataract, the rate at which the soluble lens proteins convert to insoluble is significantly increased.

Steroids are hormones that are used in some drugs and unfortunately they can also induce cataracts [35] . The mechanisms are unclear. The cataract develops gradually, starting with a Y-suture dissociation and light scattering in the posterior supranuclear region at the third month and spreads to the anterior lenticular cortex at the eight

[1]Brunescent cataracts are numclear cataracts with significant increase in the pigment levels

month. At the tenth month there are posterior subcapsular opacities formed.

The eye lens is constantly nourished by the aqueous humor. The aqueous can contain chemicals which are harmful for its normal function. In particular, a cataract can develop if a high concentration of sugars is present. Such cataracts are the sugar cataracts. Glucose is transformed to sorbitol which cannot go back through the capsule and remains in the lens, creating an osmotic gradient. As a consequence, the fibers hydrate, swell and separate [1]. Another metabolic cataract is associated with the Wilson's disease. It is characterized with copper deposits in the lens capsule and the Descement's membrane.

A trauma can also be a reason for the development of a cataract later in life. Perforation, dislocation, damage of individual fibers, totally or partially leads to change in the optical properties of the eye lens [1].

1.4 Cataract Classification

There does not exist an worldwide accepted system of classification of cataracts, but there are some factors, which play a role in a possible classification - age of the person, location, degree of progression, rate of the progression, biomicroscopic appearance and etiology. According to the age at which the cataract has appeared, we distinguish congenital, infantile, juvenile, adult and senile. The location at which the cataract appears provides other descriptive names. We have nuclear, cortical, capsular (posterior or anterior) and subcapsular (posterior or anterior). Some of them and their locations are

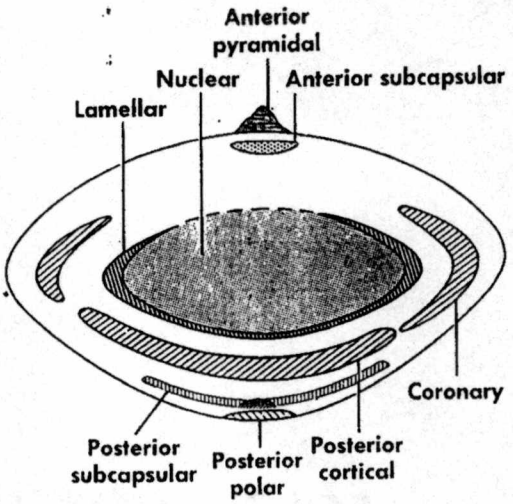


Figure 1.3: Types of cataracts depending on their location.

shown on Fig.1.3. The degree of progression is another descriptive factor: immature cataracts (transparent lens fibers are present), intumescent cataracts (swelling of lens with fluid clefts), mature cataracts (opaque lens), hypermature cataracts (liquefaction of the opaque lens fibers) and after-cataracts, which appear after the lens has been removed. A cataract is stationary if no progression has been noticed and progressive otherwise. According to the way the cataract appears microscopically, it is lamellar, coralliform and others. The etiological classification is more complicated. It describes the eye condition depending on the presence or the absence of other disorders of the eye: systematic or nonsystematic. Nearly all senile, adult, hereditary and congenital cataracts are in the group of "eye otherwise healthy and no systematic disease". Cataracts, which are combined with other ocular, systematic diseases are embriopathy, Marfan syndrome, retinal pigment epithelium and others.

A group led by J. M. Sparrow, A. J. Bron and N. A. P. Brown developed the Oxford Clinical Cataract Classification and Grading System (OCCCGS). The ambition was to make a classification system which will grade features like anterior subcapsular clear zone thickness, anterior subcapsular opacity, posterior subcapsular opacity, cortical spoke opacity, water clefts, vacuoles, retro-dots, focal dots, nuclear brunescence and white nuclear scatter. These features are graded according to their properties. For example, vacuoles are graded according to their frequency within a 8mm diameter and nuclear brunescence is graded by comparison with standard Munsell color samples [36]. The quality of the image in the presence of cataract is evaluated by the use of a resolution test target projection ophthalmoscope. The image of the chart is projected into the patients eye occupying 3 mm of the pupil. Cataracts degrade the image both during projection and visualization of the target. Since the capabilities of the photographic methods vary for visualizing different cataract types or lens features, the Oxford group suggests the they are combined for better evaluation [37, 38, 39, 40, 41].

Another classification system for cataracts was developed by the Japanese Cooperative Cataract Epidemiology Study Group (JCCESG). The eye lenses are examined using a retroillumination photography. Three major cataract types are distinguished in this study: cortical, nuclear and subcapsular. The cataract progression is divided into three stages (grades) such as Grade I (early stage), Grade II (moderate stage) and Grade III (advanced stage). In case of cortical opacities Grade I is given if the opacity covers less then 20 per cent of the pupillary area. Grade II corresponds to an opacity covering 20

to 60 per cents of the pupil area and Grade III is an opacity covering more than 60 per cents of the area. Nuclear opacities are evaluated by the scattering intensities observed with a slit lamp. The pictures taken with a Scheimpflug camera are examined using densitometric analysis. Subcapsular opacities are judged by the size of the opaque area. Grade I is a cataract covering an area as large as the pupil. If a cataract is larger than a normal pupil but smaller than a moderately dilated pupil, it is classified as Grade II. If it appears larger than that, it is given a Grade III. This research group also provided a chart for a better documentation of the cataract changes.

Sasaki found the classification system provided by the OCCCGS and the JCCESG to be insufficient for nuclear cataracts. He developed a classification system that is based in part on information of the appearance of the borders of the inner and outer fetal nuclei, light scattering intensity in the nuclear area and coloration of the nuclei and so on. The classification is done using Scheimflug photography. In this system, a Grade I cataract describes the initial phase of the cataract formation. The fetal nucleus is not easily seen, unlike the adult portion. Further, the light scattered from the anterior and posterior part of the nuclei is equal. Grade II is the next phase, in which no border is visible; the nuclear shape is visible; the posterior nucleus is darker. Grade III - the fetal nuclei is not defined; there is highly scattered intensity from the nucleus, and a yellowish color is observed on the posterior part. Grade IV - the nucleus cannot be seen, and the posterior part is difficult to observe. To clarify the difference between an early stage of nuclear cataract from normal ageing of the subject eyes he gave an

objective dependence of the transparency of the eye lens versus the age Fig1.4. Sasaki believes that a combination of the grade of the nuclear opacity, light transmittance through the lens nuclei and the visual function Fig1.4 gives an objective measure for the cataract progression and type. This system is called Kanazawa Medical University Nuclear Cataract Classification System.

The cataract classification system of The Age Related Eye Disease Study (AERDS) is based on standard photographs of lens, with Grades A through G describing no lens opacity to severe opacity, respectively. The grading is based on the area of the lens involvement in the posterior and subcapsular opacities and the optical density of nuclear opacities [42].

The America Cooperative Cataract Research Group (CCRG) has used a method to classify lens opacifications. The eye lens is split into four zones (subcapsular, cortical, supranuclear, and nuclear). Specific terminology is introduced for different features of the cataract as follows: I (immature) is a cataract which does not cover all the anatomical regions in the lens; M (mature) in which the anatomical zones are not recognizable; H (hypermature) is characterized by swelling and an increase in the anterior-posterior thickness; CXA means anterior cortex etc. I-CXA, for example, means immature cortical cataract in the anterior. For a more detailed study of the opacities, the volume of each quadrant was calculated [43].

For more information on cataract classifications see [37, 38, 39, 40, 41, 42, 43, 44, 45].

All the classifications presented so far give a description of the cataracts, but there

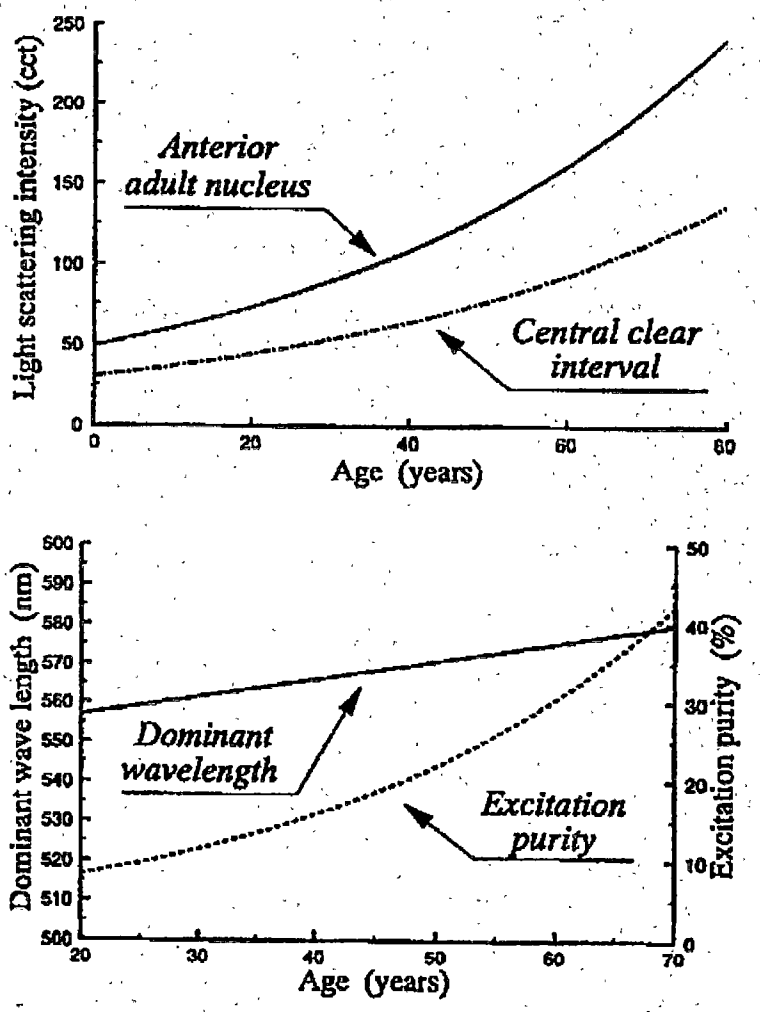


Figure 1.4: Lens transparency decrease (up) and lens coloration changes (down) of noncataractous eyes with age [9].

is no quantitative description of the volume and the number density of the cataracts. It is not quite clear how large is the early cataract and when a certain condition is pre-cataractous. In Chapter 4 a method for determination of the size distribution functions of small cataract particles is described. This method is also capable in measuring the number density of the cataracts, which can be a good quantitative description of the cataract progression. Further, both features are required to define the visual acuity of the patient. Opacities depend on the particle size distribution and the index of refraction. An image of the opacity alone does not enable an accurate prediction of the visual perception and acuity of the subject.

1.5 Pediatric Cataracts

Pediatric cataracts appear in early childhood and are normally a result from a genetic disorder, infection during pregnancy, genetic disorder or a mechanical injury. It can also accompany other disorders, such as Rubella Syndrome, for example. Descriptions of pediatric cataracts are given in Table1.1.

Table 1.1: Description of pediatric cataracts [1].

Type	Description	Details
Nuclear	Involving or central to the Y suture	Indicates that the cataract was present at birth
Cortical - lamellar	Peripheral to the Y - suture	Layered in an onion-like layer pattern; indicates a metabolic disease
Anterior		
-anterior polar	Spreads onto the anterior capsule and anterior cortex at the pole of the lens	Small, nonprogressive, does not interfere with visual acuity (in general)
-anterior subcapsular	Appears under the anterior capsule in the anterior lens cortex	Associated with neurosensory hearing loss and hemorrhagic nephritis with later retinal failure
Posterior		
-posterior lenticonus	Congenital thinning and Posterior bowing of the posterior capsule	Cortex is clear at infancy,then progresses
-persistent hyperplastic primary vitreous (PHPV)	Abnormal regression of the primitive hylaloid vascular system. This produces a fibrovascular tissue that emanates from the optic disc as a stalk, and courses to the back of the lens, where it forms a retrolental membrane	If left untreated, severe forms of PHPV can lead to shallowing of the anterior chamber, angle-closure glaucoma, and eventual loss of the eye
-posterior subcapsular	Appears at the posterior lens cortex	May be adiopatic or associated with Down's syndrome, chronic steroid use, or blunt trauma
-oil-drop	A Faint opacity in the central part of the posterior cortex	Associated with galactosemia
-Christmas tree	Contains multiple small flecks of various colors	Associated with myopic dystrophy, pseudohypoaparathyroidism, hypoparathyroidism
Cerulean	A blue-dot cataract. Consists of multiple small opacities, scattered within the cortex, which are bluish white in color	Down's syndrome or may be idiopathic, occurring during early puberty. Usually causes minimal loss
Membranous	The cortex has been absorbed and the anterior capsule come in close proximity. There can be calcification in the lens capsule bag	Can be a consequence of a trauma, intrauterine infections or anomalous lens development, because of genetical disorder of the anterior chamber

Table 1.2: Average annual number of cataracts (in thousands), by age, race and geographic location. Bold numbers show the rate per thousand [2, 3, 4, 5, 6, 7].

		Gender			Race			Region			
Age	Period	Both	Male	Female	All	White	Black	Northwest	Midwest	South	West
All	1982-84	7,984	1,631	6,353	7,984	4,560	341	-	-	-	-
		21.7	**14.7**	**28.3**	**21.7**	**23.3**	**12.5**	-	-	-	-
55-64		677	279	398	677	897	56	-	-	-	-
		30.8	**27.2**	**33.9**	**30.8**	**30.3**	**28.5**	-	-	-	-
65-74		1,516	439	1,077	1,516	1,394	117	-	-	-	-
		94.4	**63.0**	**118.5**	**94.4**	**96.3**	**86.8**	-	-	-	-
75-84		1,739	491	1,249	1,739	1,615	90	-	-	-	-
		217.8	**162.6**	**251.4**	**217.8**	**223.0**	**138.2**	-	-	-	-
85 and		611	169	442	-	-	-	-	-	-	-
older		-	-	-	-	-	-	-	-	-	-
All	1985-87	5,481	1,761	3,719	5,481	4,912	453	-	-	-	-
		23.2	**15.4**	**30.5**	**23.2**	**24.5**	**15.9**	-	-	-	-
55-64		739	292	448	739	645	54	-	-	-	-
		33.6	**28.2**	**38.4**	**33.6**	**33.1**	**25.9**	-	-	-	-
65-74		584	239	345	1,681	1,475	167	-	-	-	-
		98.9	**71.3**	**120.6**	**98.9**	**96.5**	**114.7**	-	-	-	-
75-84		1,994	517	1,477	1,994	1,831	137	-	-	-	-
		233.7	**160.8**	**227.8**	**233.7**	**237.2**	**198.1**	-	-	-	-
85 and		619	163	456	-	-	-	-	-	-	-
older		-	-	-	-	-	-	-	-	-	-
All	1988-90	5,910	1,888	4,022	5,910	5,361	491	-	-	-	-
		24.3	**16.0**	**32.0**	**24.3**	**26.1**	**16.4**	-	-	-	-
55-64		698	313	385	698	609	77	-	-	-	-
		32.6	**30.9**	**34.0**	**32.6**	**32.5**	**36.4**	-	-	-	-
65-74		2,006	677	1,329	2,006	1,842	145	-	-	-	-
		112.5	**85.3**	**134.3**	**112.5**	**115.3**	**94.1**	-	-	-	-
75-84		2,026	524	1,502	2,026	1,847	160	-	-	-	-
		221.0	**149.2**	**265.6**	**221.0**	**222.2**	**218.8**	-	-	-	-
85 and		626	151	475	-	-	-	-	-	-	-
older		-	-	-	-	-	-	-	-	-	-
All	1989-91	6,070	1,953	4,117	6,070	5,500	521	-	-	-	-
		24.7	**16.4**	**32.5**	**24.7**	**26.6**	**17.2**	-	-	-	-
55-64		688	271	416	688	592	80	-	-	-	-
		32.3	**27.0**	**37.1**	**32.3**	**31.9**	**37.4**	-	-	-	-
65-74		2,093	706	1,387	2,093	1,919	155	-	-	-	-
		115.8	**87.5**	**138.6**	**115.8**	**118.7**	**98.6**	-	-	-	-
75-84		2,143	606	1,537	2,143	1,959	173	-	-	-	-
		228.6	**167.5**	**267.0**	**228.6**	**230.6**	**229.9**	-	-	-	-
85 and		566	138	427	-	-	-	-	-	-	-
older		-	-	-	-	-	-	-	-	-	-
All	1990-92	6,411	2,146	4,265	6,411	5,758	574	1,257	1,692	2,314	1,153
		25.8	**17.8**	**33.3**	**25.8**	**27.6**	**18.6**	**25.1**	**28.0**	**27.5**	**21.3**
55-64		816	291	525	816	695	110	-	-	-	-
		38.6	**29.0**	**47.1**	**38.6**	**37.8**	**50.8**	-	-	-	-
65-74		2,231	815	1,416	2,231	2,065	147	-	-	-	-
		122.0	**99.7**	**140.1**	**122.0**	**126.6**	**91.6**	-	-	-	-
75-84		2,129	623	1,507	2,129	1,919	186	-	-	-	-
		232.2	**166.9**	**259.3**	**223.2**	**221.9**	**246.3**	-	-	-	-
85 and		617	163	454	-	-	-	-	-	-	-
older		-	-	-	-	-	-	-	-	-	-
All	1993	6,067	under 45	under 45	-	under 45	under 45	1,284	1,272	2,356	1,156
		23.9			-			**25.7**	**20.5**	**27.6**	**20.3**
younger		55	219	112	-	261	70	-	-	-	-
then 18		**0.8**	**2.5**	**1.3**	-	**1.9**	**2.9**	-	-	-	-
18-44		276			-			-	-	-	-
		2.6			-			-	-	-	-
45-64		996	329	668	-	788	188	-	-	-	-
		20.0	**13.7**	**25.9**	-	**18.4**	**36.6**	-	-	-	-
65-74		2,122	728	1,394	-	1,945	165	-	-	-	-
		114.0	**87.1**	**135.9**	-	**117.7**	**98.6**	-	-	-	-
75 and		2,617	665	1,952	-	2,305	270	-	-	-	-
older		**206.8**	**139.4**	**247.6**	-	**201.7**	**270.3**	-	-	-	-
All	1994	6,473	under 45	under 45	-	under 45	under 45	1.213	1,507	2,434	1,318
		24.9			-			**24.0**	**23.8**	**27.6**	**22.8**
younger		96	222	222	-	401	42	-	-	-	-
then 18		**1.4**	**2.5**	**2.5**	-	**2.8**	**1.7**	-	-	-	-
18-44		347			-			-	-	-	-
		3.2			-			-	-	-	-
45-64		872	299	572	-	739	86	-	-	-	-
		17.3	**12.3**	**21.9**	-	**17.1**	**16.8**	-	-	-	-
65-74		2,062	641	1,420	-	1,839	178	-	-	-	-
		113.0	**79.0**	**140.0**	-	**113.6**	**114.6**	-	-	-	-
75 and		3,096	1,035	2,061	-	2,751	280	-	-	-	-
older		**242.4**	**214.7**	**259.2**	-	**237.9**	**288.4**	-	-	-	-

Table 1.3: Average annual number of cataracts (in thousands), by age, race and geographic location. Bold numbers show the rate per thousand [2, 3, 4, 5, 6, 7]

		Gender			Race			Region			
Age	Period	Both	Male	Female	All	White	Black	Northwest	Midwest	South	West
All	1982-84	7,984	1,631	6,353	7,984	4,560	341	-	-	-	-
		21.7	**14.7**	**28.3**	**21.7**	**23.3**	**12.5**	-	-	-	-
55-64		677	279	398	677	897	56	-	-	-	-
		30.8	**27.2**	**33.9**	**30.8**	**30.3**	**28.5**	-	-	-	-
65-74		1,516	439	1,077	1,516	1,394	117	-	-	-	-
		94.4	**63.0**	**118.5**	**94.4**	**96.3**	**86.8**	-	-	-	-
75-84		1,739	491	1,249	1,739	1,615	90	-	-	-	-
		217.8	**162.6**	**251.4**	**217.8**	**223.0**	**138.2**	-	-	-	-
85 and		611	169	442	-	-	-	-	-	-	-
older		-	-	-	-	-	-	-	-	-	-
All	1985-87	5,481	1,761	3,719	5,481	4,912	453	-	-	-	-
		23.2	**15.4**	**30.5**	**23.2**	**24.5**	**15.9**	-	-	-	-
55-64		739	292	448	739	645	54	-	-	-	-
		33.6	**28.2**	**38.4**	**33.6**	**33.1**	**25.9**	-	-	-	-
65-74		584	239	345	1,681	1,475	167	-	-	-	-
		98.9	**71.3**	**120.6**	**98.9**	**96.5**	**114.7**	-	-	-	-
75-84		1,994	517	1,477	1,994	1,831	137	-	-	-	-
		233.7	**160.8**	**227.8**	**233.7**	**237.2**	**198.1**	-	-	-	-
85 and		619	163	456	-	-	-	-	-	-	-
older		-	-	-	-	-	-	-	-	-	-
All	1988-90	5,910	1,888	4,022	5,910	5,361	491	-	-	-	-
		24.3	**16.0**	**32.0**	**24.3**	**26.1**	**16.4**	-	-	-	-
55-64		698	313	385	698	609	77	-	-	-	-
		32.6	**30.9**	**34.0**	**32.6**	**32.5**	**36.4**	-	-	-	-
65-74		2,006	677	1,329	2,006	1,842	145	-	-	-	-
		112.5	**85.3**	**134.3**	**112.5**	**115.3**	**94.1**	-	-	-	-
75-84		2,026	524	1,502	2,026	1,847	160	-	-	-	-
		221.0	**149.2**	**265.6**	**221.0**	**222.2**	**218.8**	-	-	-	-
85 and		626	151	475	-	-	-	-	-	-	-
older		-	-	-	-	-	-	-	-	-	-
All	1989-91	6,070	1,953	4,117	6,070	5,500	521	-	-	-	-
		24.7	**16.4**	**32.5**	**24.7**	**26.6**	**17.2**	-	-	-	-
55-64		688	271	416	688	592	80	-	-	-	-
		32.3	**27.0**	**37.1**	**32.3**	**31.9**	**37.4**	-	-	-	-
65-74		2,093	706	1,387	2,093	1,919	155	-	-	-	-
		115.8	**87.5**	**138.6**	**115.8**	**118.7**	**98.6**	-	-	-	-
75-84		2,143	606	1,537	2,143	1,959	173	-	-	-	-
		228.6	**167.5**	**267.0**	**228.6**	**230.6**	**229.9**	-	-	-	-
85 and		566	138	427	-	-	-	-	-	-	-
older		-	-	-	-	-	-	-	-	-	-
All	1990-92	6,411	2,146	4,265	6,411	5,758	574	1,257	1,692	2,314	1,153
		25.8	**17.8**	**33.3**	**25.8**	**27.6**	**18.6**	**25.1**	**28.0**	**27.5**	**21.3**
55-64		816	291	525	816	695	110	-	-	-	-
		38.6	**29.0**	**47.1**	**38.6**	**37.8**	**50.8**	-	-	-	-
65-74		2,231	815	1,416	2,231	2,065	147	-	-	-	-
		122.0	**99.7**	**140.1**	**122.0**	**126.6**	**91.6**	-	-	-	-
75-84		2,129	623	1,507	2,129	1,919	186	-	-	-	-
		232.2	**166.9**	**259.3**	**223.2**	**221.9**	**246.3**	-	-	-	-
85 and		617	163	454	-	-	-	-	-	-	-
older		-	-	-	-	-	-	-	-	-	-
All	1993	6,067	under 45	under 45	-	under 45	under 45	1,284	1,272	2,356	1,156
		23.9			-			**25.7**	**20.5**	**27.6**	**20.3**
younger		55	219	112	-	261	70	-	-	-	-
then 18		**0.8**	**2.5**	**1.3**	-	**1.9**	**2.9**	-	-	-	-
18-44		276			-			-	-	-	-
		2.6			-			-	-	-	-
45-64		996	329	668	-	788	188	-	-	-	-
		20.0	**13.7**	**25.9**	-	**18.4**	**36.6**	-	-	-	-
65-74		2,122	728	1,394	-	1,945	165	-	-	-	-
		114.0	**87.1**	**135.9**	-	**117.7**	**98.6**	-	-	-	-
75 and		2,617	665	1,952	-	2,305	270	-	-	-	-
older		**206.8**	**139.4**	**247.6**	-	**201.7**	**270.3**	-	-	-	-
All	1994	6,473	under 45	under 45	-	under 45	under 45	1.213	1,507	2,434	1,318
		24.9			-			**24.0**	**23.8**	**27.6**	**22.8**
younger		96	222	222	-	401	42	-	-	-	-
then 18		**1.4**	**2.5**	**2.5**	-	**2.8**	**1.7**	-	-	-	-
18-44		347			-			-	-	-	-
		3.2			-			-	-	-	-
45-64		872	299	572	-	739	86	-	-	-	-
		17.3	**12.3**	**21.9**	-	**17.1**	**16.8**	-	-	-	-
65-74		2,062	641	1,420	-	1,839	178	-	-	-	-
		113.0	**79.0**	**140.0**	-	**113.6**	**114.6**	-	-	-	-
75 and		3,096	1,035	2,061	-	2,751	280	-	-	-	-
older		**242.4**	**214.7**	**259.2**	-	**237.9**	**288.4**	-	-	-	-

		Gender			Race			Region			
Age	Period	Both	Male	Female	All	White	Black	Northwest	Midwest	South	West
All	1995	6,256	under 45	under 45	-	under 45	under 45	1.027	1,523	2,399	1,318
		23.9			-			**20.0**	**24.5**	**26.0**	**23.4**
younger		14	78	117	-	194	42	-	-	-	-
then 18		**0.2**	**1.8**	**1.1**	-	**1.3**	**1.7**	-	-	-	-
18-44		249			-			-	-	-	-
		2.3			-			-	-	-	-
45-64		998	209	426	-	827	86	-	-	-	-
		19.3	**16.8**	**21.6**	-	**18.7**	**16.8**	-	-	-	-
65-74		1,945	311	445	-	1,729	178	-	-	-	-
		105.4	**72.1**	**132.1**	-	**106.3**	**114.6**	-	-	-	-
75 and		3,050	403	489	-	2,813	280	-	-	-	-
older		**234.5**	**214.0**	**247.0**	-	**237.9**	**16.0**	-	-	-	-
All	1996	7,022	under 45	under 45	-	under 45	under 45	1.153	1,845	2,419	1,605
		26.6			-			**21.4**	**29.1**	**26.7**	**28.5**
younger		33	141	192	-	264	42	-	-	-	-
then 18		**0.5**	**1.6**	**2.1**	-	**1.8**	**1.7**	-	-	-	-
18-44		299			-			-	-	-	-
		2.8			-			-	-	-	-
45-64		1,240	444	796	-	1,083	86	-	-	-	-
		23.3	**17.3**	**29.6**	-	**23.7**	**16.8**	-	-	-	-
65-74		2,796	899	1,898	-	2,506	178	-	-	-	-
		151.9	**109.3**	**186.4**	-	**153.7**	**114.6**	-	-	-	-
75 and		2,653	967	1,685	-	2,486	280	-	-	-	-
older		**198.6**	**189.6**	**203.9**	-	**202.9**	**182.0**	-	-	-	-

Chapter 2

Techniques for Cataract Diagnosis

2.1 Slit Lamp

Slit lamps are the most common opthalmic instruments used to diagnose most of the eye diseases, including cataracts. They consist of a light source (normally a 20-50W halogen lamp) and a biomicroscope (magnification up to 40X), which during the examination are swung around the eye. According to [10], using auxiliary devices, the slit lamp is capable of measuring intraocular pressure, endothelial cell counts, pupil size, corneal thickness, anterior chamber depth and photographic recording. It has an illumination and observation system. A basic slit lamp is shown on Fig.2.1.

Different abnormalities of the eye appear in different sizes, shapes, textures and

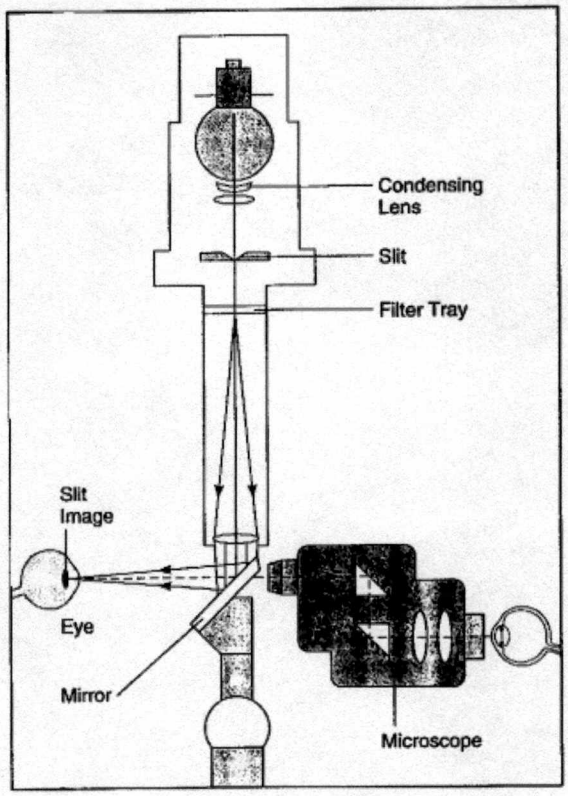


Figure 2.1: Diagram of a slitlamp [10].

depths. Therefore, different methods of illumination are necessary to visualize them. To do so, the size of the slit (the beam), the angle of view, the light source color temperature, the exposure time can be varied. Some structures appear better if they are illuminated with a certain wavelength, for which a set of filters is available.

The higher the color temperature of the light source, the higher the blue component of the light [10]. Those wavelengths are comparable to the size of the objects, which makes them easier to observe. The larger the angle of illumination, the more surface details can be viewed, because of the shadow patterns appearing on the surface [10, 46].

There are two types of microscopes used in a combination with the slit lamp: the clinical biomicroscope and the photographic microscope. The photographic microscope

differs by having a beam splitter which delivers part of the reflected light to the camera and part of the light to the eye of the observer. Another feature of this microscope is the synchronized flash illuminator, which allows the camera to record exactly what is viewed at the moment.

The slit lamp has been very useful for cataract diagnosis and visualization. It is used in all the ophthalmological offices, as well as in the development of cataract classification systems. If the recording is done according to the Scheimflug principle, the technique can give information for the volume of the cataracts [47]

2.2 Optical Coherence Tomography

The method of Optical Coherence Tomography (OCT) is becoming very popular, because it is capable of acheiving less then 20 μm resolution. Opportunities for visualizing cataracts using OCT are pointed out by [48, 49].

This method takes advantage of the coherence length of a broadband light source. The light illuminates both the reference mirror and the tissue [50, 51, 49, 48]. Then, the reflected beam from the mirror and the transmitted beam from the sample are combined. Interference signal will be detected only if the path difference of the two beams is less then the coherence length of the light source. A two-dimensional picture of the tissue is obtained by scanning the reference mirror.

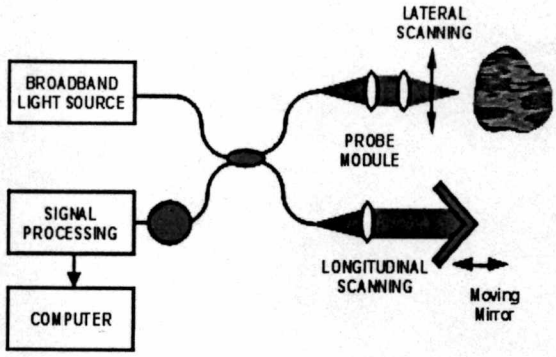


Figure 2.2: Schematic of an optical coherence tomography system [11].

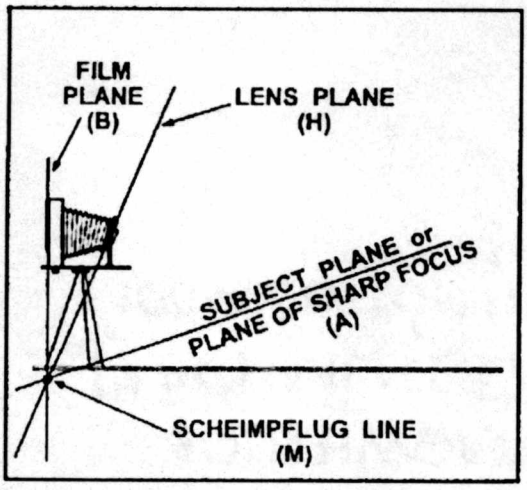


Figure 2.3: Illustration of the Scheimflug principle [12].

2.3 Scheimflug Photography

The Scheimflug photography is widely used in opthalmology for visualization and classification of cataracts [52, 47, 53, 54]. It is based on the Sheimflug principle, which states that the quality of the picture improves if the planes of the lens, object and photographic plate are intersected in a line (Fig.2.3)[55, 12].

An instrument which has been used for a three dimensional reconstruction of the cataracts is the Anterior Segment Analysis System (Nidek, EAS-1000)[52, 47]. It has a CCD camera with a computer analysis system. The camera was rotated about the axis of the patient's eye lens in increment of 3 degrees to obtain 60 images to obtain 60 images. Then the images were processed to obtain the volume of the cataracts. The advantages of this method are that it uses a new interpolation procedure for the volume reconstruction; uses an easy to use software and represents the lens in pseudocolors. The disadvantage is that the camera had to be rotated manually, which takes a lot of time (about 20 min), which is not acceptable in a normal ophthalmological test. This problem was overcome by Peter Egner [56]. He automated the rotation of the camera by the use of an angle detector attached to the CCD camera (Fig.2.4)

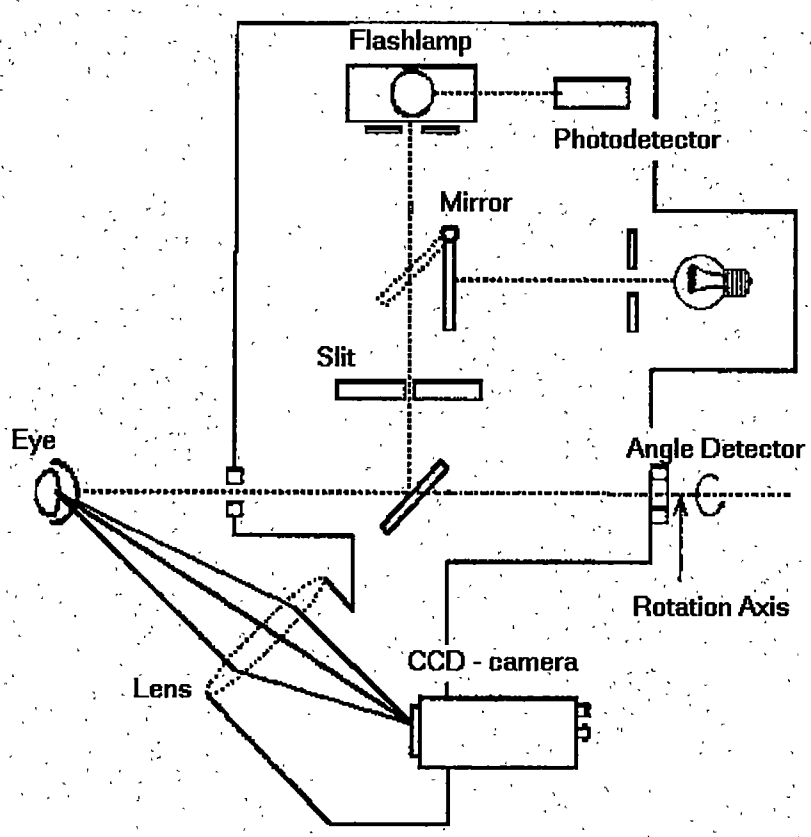


Figure 2.4: Scheimflug slit lamp with a CCD camera [12].

Chapter 3

The Eye Lens

3.1 Normal Eye Lens

The human lens is a transparent double-convex shaped body that is seated anteriorly to the vitreous and posteriorly to the aqueous and the iris . Together with the cornea and the retina it completes the optical system of the eye. Its optical power can change with the help of the ciliary muscle. The process is called accommodation.

The three components of the lens are nucleus, cortex and capsule. The nucleus is positioned in the center and it is the oldest part of the tissue (see Fig.3.1). The embryonic part of the nucleus is the first one to form in the human's eyes and through the microscope, it appears like a dark vertical bar in the center of the lens. It is surrounded by a shell, called fetal nucleus, which is characterized by the specific Y-sutures on the boundaries.They are symmetrical and inverted on both sides [21]. The infantile and the adult nuclei are not easily distinguished before the age of 35 to 40

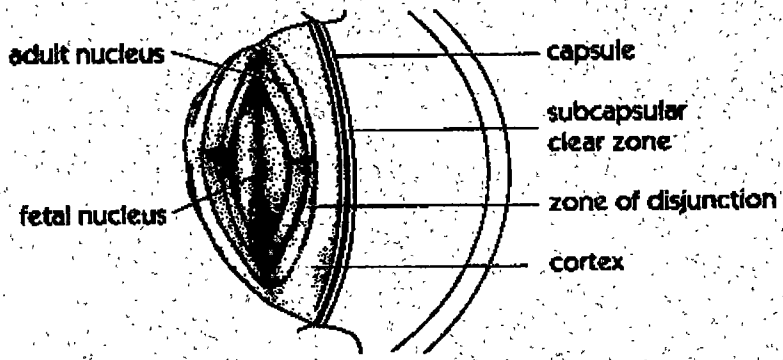


Figure 3.1: Layers of the eye lens [10].

years. The capsule is a membranous tissue which surrounds the lens and is more flat in front than in the back [57]. Its thickness varies from 4μm to 23μm [22].

Two cell types are represented in the eye lens - epithelial cells on the anterior surface, under the capsule, and fiber cells, which occupy the rest of the lens. The epithelial cells undergo mitosis and subsequently differentiate into the fiber cells. The new fiber cells are laid down as concentric layers on previously formed embryonic fibers. With time, they are compressed tighter and more inward. The number of fiber cells increases from 1,662,010 at birth to 3,546,100 at the age of 80 years. Typical young adult fibers may be about 2μm thick, 10-12μm wide and can be as long as 7-10mm [21]. The fiber cells run from the anterior to the posterior pole of the lens, attaching at the sutures. Each fiber runs completely around from the front of the lens to the back [57]. The ends of the fibers join to form sutures on both sides of the lens with the shape of the letter "Y" - the Y-sutures. The protein turnover is very little in the nucleus. Most of the protein is synthesized in the epithelium or in the fiber cells in the peripheral cortex. That is why the mass of the eye lens changes from 65mg at birth to about 250mg at age of 90 years [21].

3.2 Eye Lens Proteins

Three types of structural proteins comprise the lens: the cytoskeletal proteins, the membrane proteins and crystallins. Ninety percent of the total dry mass of the eye lens is made up from crystallin proteins [10]. They are responsible for the optical properties of the tissue and the cell functions. About thirty percent of the proteins are concentrated in the peripheral zone, while more than seventy percent are in the central area (Phillipson, 1969). The most common crystallins are the α-, β-, and γ-crystallins, which form 2 large superfamilies - a and bg. They are not evenly distributed in the lens, but their concentration increases from the periphery to the nucleus. The protein turnover is very low or absent in the eye lens, and the same is true for the mechanisms against the posttranslational modifications and protein unfolding. The transparency is maintained by the use of the chaperone properties of the α-crystallin.

3.3 α Crystallin

The α-crystallin is the most abundant (up to forty percent of total proteins [58]) and the largest protein in the fiber cells [59, 28]. Its major function is to maintain proper refractive index in the lens, but it also maintains transparency due to its chaperon-like properties. This property enables it to restrain the unfold or denaturated proteins and to suppress aggregation, which leads to cataract formation. Another interesting property is that the molar ratio of $\alpha A : \alpha B$ in the lens is 3:1 [59, 58], which is optimal for the thermal stability of this protein. There is evidence, that a-crystallin plays a



Figure 3.2: The structure of the alpha-crystallin of humans predicted by Shindyalov and Bourne based on concept of intermediate sequence search[13].

role in the epithelial cells differentiation into fiber cells [59]. α B was also found to be overexpressed in various neurodegenerative diseases and an ischemic heart.

αB is hollow with a diameter approximately 11nm. The central cavity is surrounded by a 3nm shell [58]. Since no 3-D structure of this protein was found in the Protein Data Bank or NCBI, a simulation was made using the nucleic acid sequence of the molecule (Fig.3.2)The molecular weight varies due to the heterogeneity (more than 1000 different hybrids, without including the molecules, which have undergone posttranslational modifications) of the native and recombinant crystallin. According to Horowitz, the average weight is 600,000Da to 900,000Da and the top weight measured is 1 million Da. Abraham Spector found three major populations of molecules. About 65-75%

of the total protein had a mass of 600,000Da to 900,000Da. The second group had mass range from 900,000Da to 4,000,000Da and the third group had masses larger than 1,000,000Da. Jaffe and Horowitz [21] estimated the aggregate size of αA and αB in native conditions to range from 300,000Da to 1,200,000Da with an average molecular weight of 800,000Da.

3.4 β Crystallin

$\beta\gamma$-crystallins comprise the majority of adult vertebrate lens crystallins. Beta and gamma crystallin gene families comprise the $\beta\gamma$- crystallin superfamily. All beta-crystallins have two symmetrical domains, folded into two similar patterns, called "Greek Key". Their mass vary between 50 and 200kDa. The difference between the beta- and gamma-crystallins is that the beta have N- and C- termini, while the gamma have minimal or none [60]. Although the functions of both crystallins are not quite clear, there is evidence, that beta crystallin responds to stress. It moves from the nuclear to the cytoplasmic region in case of a heat or cold shock and stabilizes the other proteins using its beta sheets and insures that the concentration of the Ca2+ is within the normal levels.

β-crystallins (Fig.3.3)comprise about thirty five percent of the total water soluble crystallin. They are built up by three acidic and three basic units called $\beta A2, \beta A3, \beta A4$, $\beta B1, \beta bB2, \beta B3$. The subunit weight ranges from 23,000Da to 200,000Da. The size of the aggregates formed in native conditions ranges from 46,000Da to 200,000Da [21].



Figure 3.3: Structure of bovine $\beta B2$ molecule [14].

The properties and the spatial distribution of the concentration of the eye lens proteins are important for maintaining the gradient of the refractive index of the eye lens and its transparency.

3.5 Transparency and Transmission of a Normal Eye Lens

Some authors argue that the transparency of the eye lens is not due to the order of the collagen molecules. Although there seem to be some kind of an order, it cannot be called a crystal. On the other hand, the index of refraction is highly dependent on the density distribution, which means that if there are more fibers or proteins in some place than another it will cause density and refractive index fluctuations. Such fluctuations

were reported to be present in the cataract formation [61].

The eye lens transmits light with wavelengths from 390nm to 1,900nm (Fig.3.4). The initial peak peak of the transmission curve is present in the lenses of young children only. Their lenses start transmitting at shorter wavelengths, but because of the strong absorption at this region, the transmission is reduced to the very low value of eight per cent for the age of 5 years and less than 0.1 per cent for the age of 22 years. The total transmission of an young eye begins to increase at about 390nm and reaches 90 per cent at about 450nm. The rate of increase is age-dependent, and it decreases in older lenses [15]. The lens is still transparent for light with wavelength about 1,400nm, and the absorption bands for water are apparent at 980nm, 1,200nm and 1,430nm.

By examining data on the color matching function of the eye Joel Pokorni [16] found out that the spectral density function of the eye lens can be decomposed into a component that is affected by aging and a component that is constant. This is expressed as:

$$T_L = T_{L_1}[1 + 0.02(A - 32)] + T_{L_2} \tag{3.1}$$

for ages between 20 and 60 years and

$$T_L = T_{L_1}[1.56 + 0.0667(A - 60)] + T_{L_2} \tag{3.2}$$

for people older than 60 years. A is the age of the person, T_{L_1} represents the portion of the transmitted light affected by aging and T_{L_2} is the portion stable after the age of 20

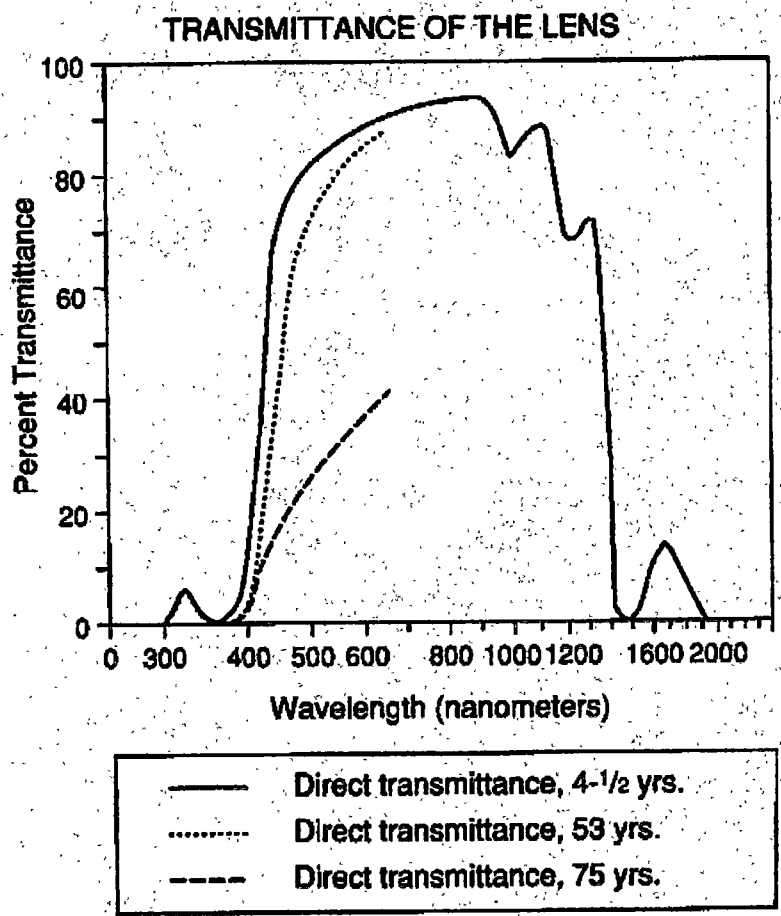


Figure 3.4: Transmission of the eye lens vs. wavelength [15].

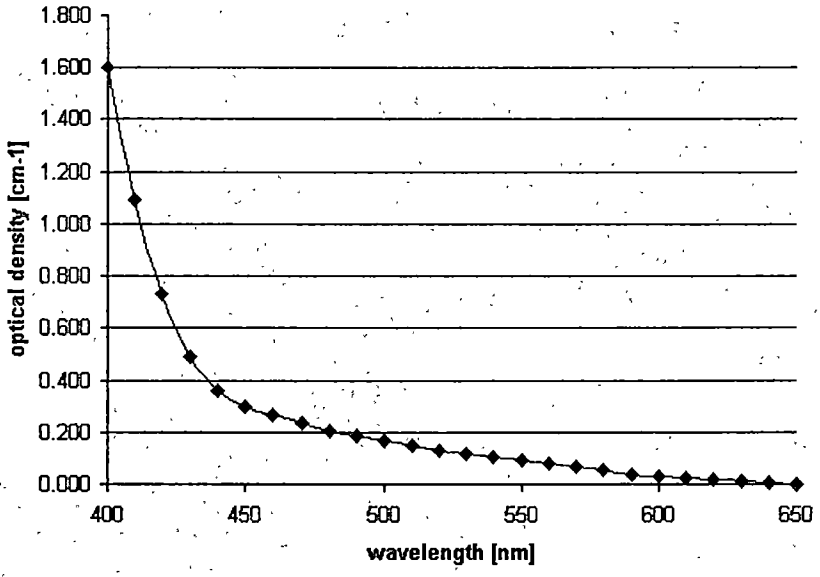


Figure 3.5: Optical density of the eye lens as a function of the wavelength. Data taken from [16].

years. The result is given in Fig.3.5.

The same kind of an idea was proposed by Hemenger [17]. He also writes the optical density function as a sum of two terms:

$$X(\lambda) = \frac{\beta}{\lambda^2} + \gamma(\lambda), \tag{3.3}$$

where the first term represents the scattering from the eye lens, which is age dependent, and $\gamma(\lambda)$ represents the contribution of the absorption in the eye lens due to the presence of lens pigments. $\gamma(\lambda)$ is considered not to give any contribution for wavelengths larger than 500nm because the pigment does not absorb in this range.

The scattering from both, the nucleus and the cortex increases with age. The scattering in the nucleus is due to density fluctuations in the refractive index due to the high

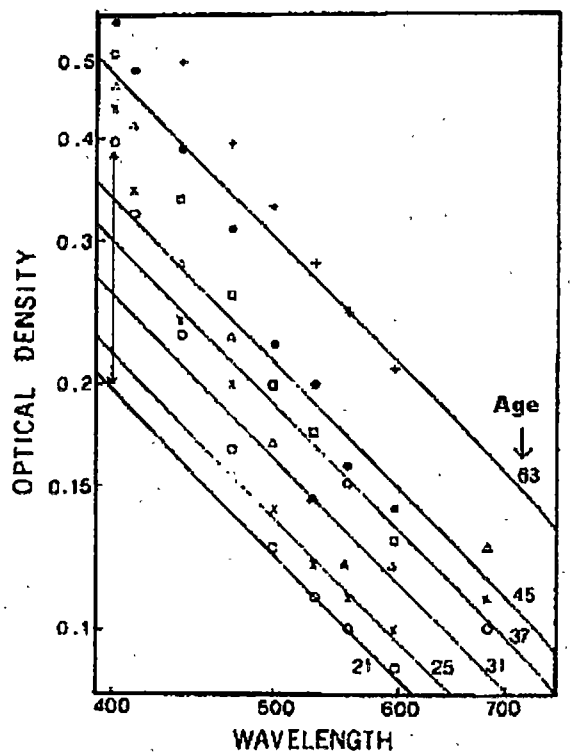


Figure 3.6: Optical density of the eye lens as a function of the age. Only the scattering term is taken into account [17].

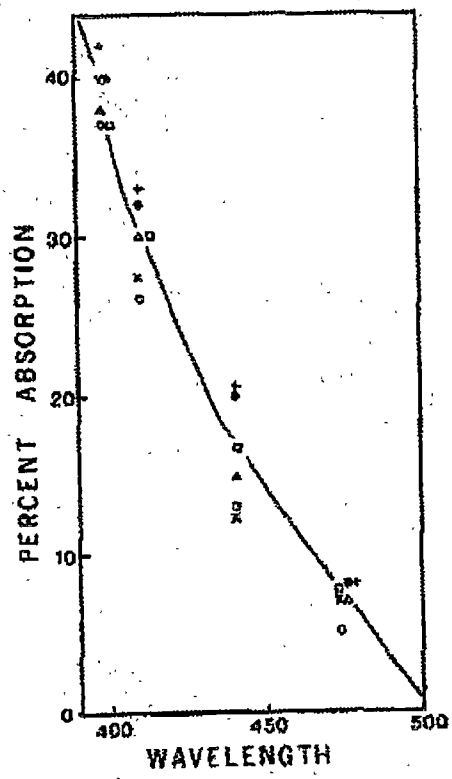


Figure 3.7: The absorption by lens pigment (in percents) as a function of age. ∘, age 21; ×, age 25; △, age 31; •, age45; and +, age 63[17].

molecular weight protein aggregation. It is not large in the young lenses, but it increases substantially after the age of 50 years. Cortical scattering, however, is constantly present in the eye lens, and it associated with a misalignment or damage of the eye lens fibers. The results from this study are given on Fig.3.6. The absorption of the eye lens pigment in absence of scattering is given on Fig.3.7. The data in this study were taken from Said and Weale [62] and Boettner[15]. The author also presents a plot for the optical density in case of a nuclear and cortical cataract using data from Ludvigh and McMarthy and Zigman et al [18, 33], Fig.3.8.

It can be seen that the optical density increases about three times in case of a cataract.

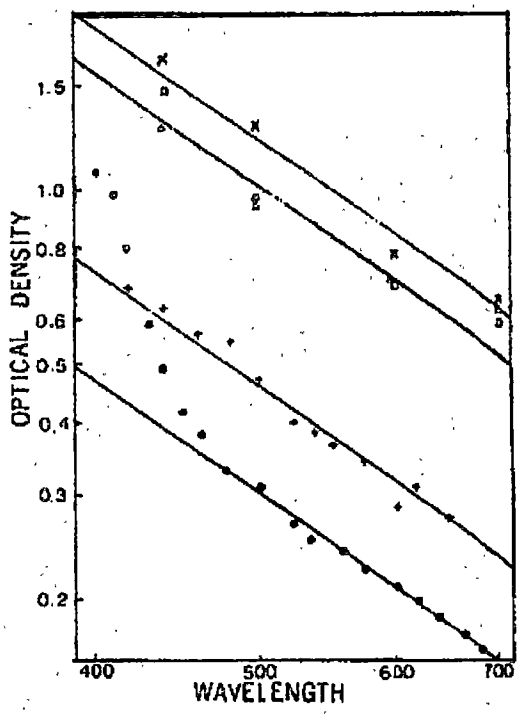


Figure 3.8: The optical density measured from different authors.o, Ludvigh and McCarthy [18]; +, Weale (a cloudy portion of a 53-years old lens)[19]; squares, Zigman et al. (cortical cataract); △, Zigman et al. (nuclear and cortical); and ×, Zigman et al. (nuclear and cortical cataract) [17].

3.6 Index of Refraction

The protein concentration distribution in the eye lens produces a gradient of the refractive index. The highest refractive power 1.407 is in the center of the nucleus where the proteins make more than 90 per cent of the dry mass. At the periphery its value is 1.36. The index of refraction distribution is also age-dependent. The refractive index distribution for two normal lenses at different ages is given on Fig.3.9. The third distribution corresponds to a lens with nucleus yellowing. As it can be seen the index of refraction can become as high as 1.45. The refractive index distribution given by Liou [63] is shown on Fig.3.10.

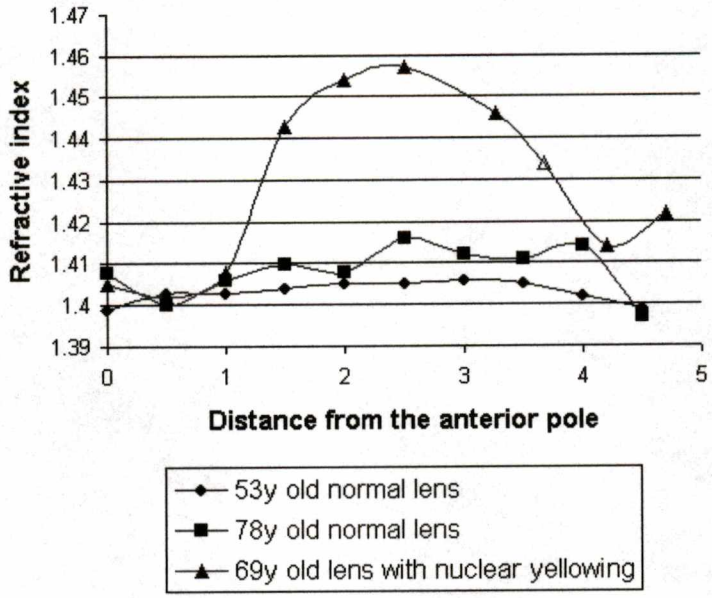


Figure 3.9: Index of refraction distribution (modified from the original)[20].

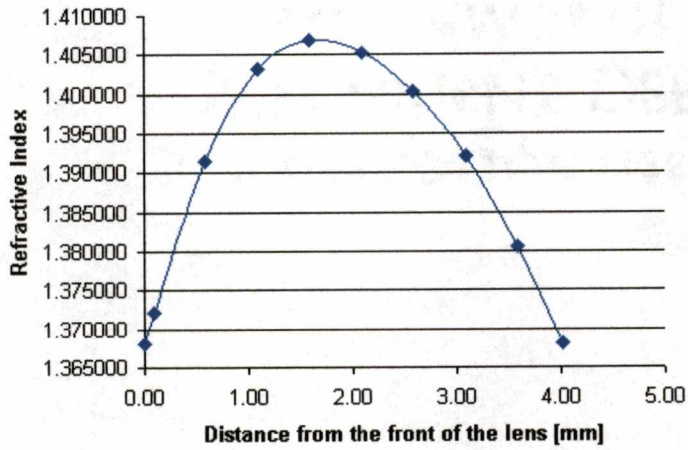


Figure 3.10: Index of refraction distribution (modified from the original)[20].

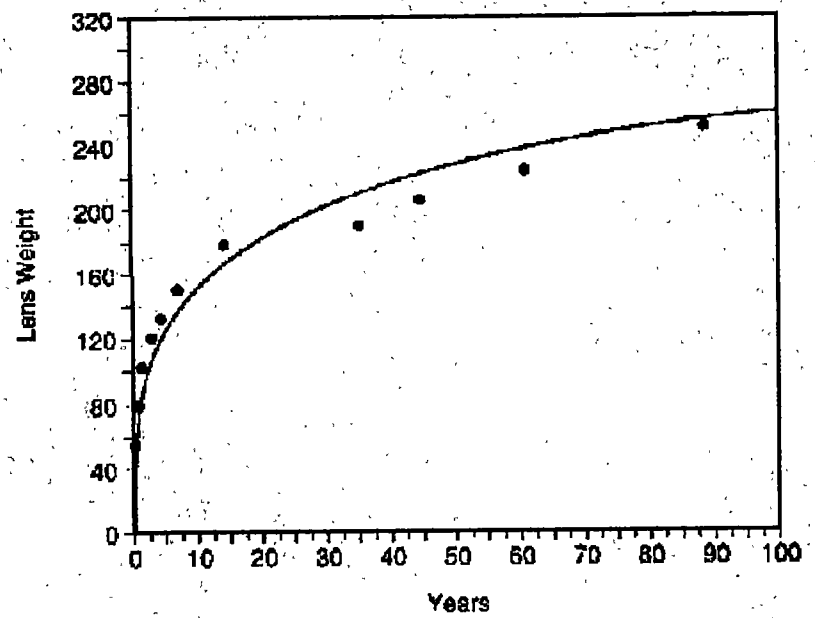


Figure 3.11: Change of the weight of the eye lens with age [21].

3.7 Aging of the Eye lens

Since there is very little or no turnover of the lens proteins, the mass [21] and the size (see Fig.3.11 and Fig.3.12)(Harding fig1.3) of the eye lens increases with the age. The mass of the eye lens increases from about 70mg in the fetal lens to about 250mg at the age of seventy years. The difference in the width over the same time interval is about 2mm. There is also an increase of light scattering and an increase in the absorption at 350nm, 400nm, 450nm, and 500nm [22, 62]. The dry mass distribution also undergoes changes (see Fig.3.13).

Biochemical changes occur in the eye lens. As a whole, the metabolic processes slow down, there are less enzyme activities and the structural proteins has undergone post-translational modifications. Another sign of aging is the degradation of all the proteins in the eye lens - crystallins, membranes and enzymes. The portion of the insoluble

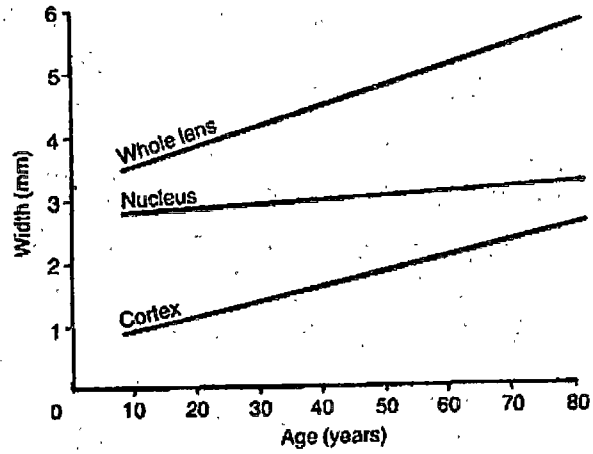


Figure 3.12: Change of the size of the eye lens with age [22].

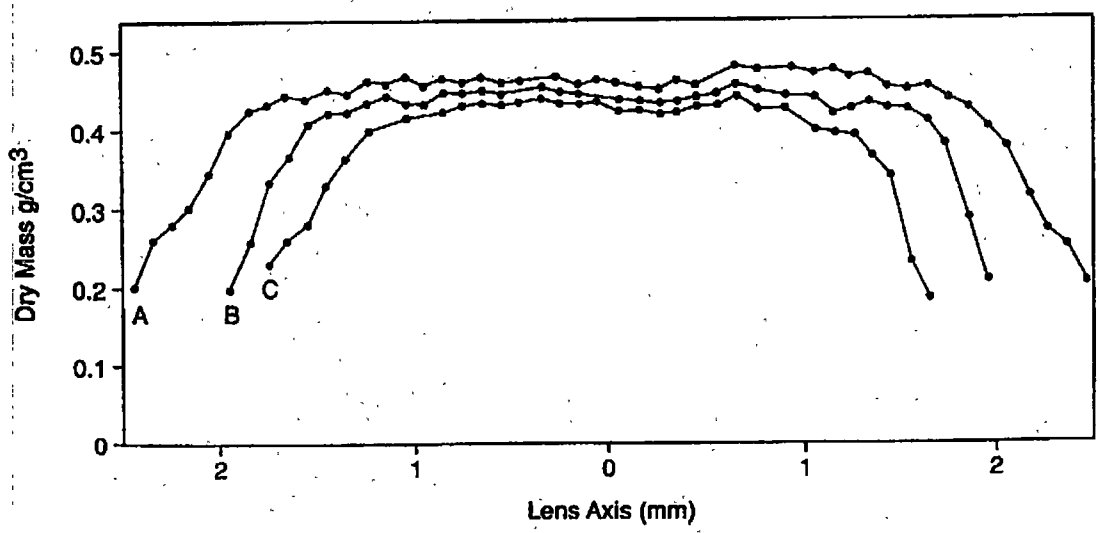


Figure 3.13: Dry mass distribution along the lens axis in three normal lenses: A, 62 years old, B, 24 years old and C, 1.5 years old[21].

proteins and the high molecular weight aggregates becomes larger, which leads to an increase of the light scattering with age. There is also a change in the relative amounts of the different types of proteins. The ratios of $\alpha B : \alpha A$ and $\gamma\delta : \gamma c$ increase [64]. Results from circular dichroism measurements have indicated that there are possible changes in the tertiary structure of α-crystallins which may be unfolding [65]. Other studies [64] have indicated that a truncation of the N-termini of the $\beta B1, \beta A3$ and $\beta A1$ occurs and that the proportion of the truncated proteins increases with age.

3.8 Cataractous Lens

As it was mentioned before the cataract formation is a consequence of variety of factors: mechanical, biochemical and radiation. These factors may affect the arrangement and the histology of the lens fibers or induce chemical changes in the proteins.

Most vulnerable to those factors are the youngest fibers, which is the reason why most of the cataracts are initiated in the subcapsular region [29]. The senile cataracts, in contrast, start from the deep cortex and the nucleus.

We call a cataract lamellar if the fibers within a particular perinuclear fiber shell are affected, and it is called a spoke if limited groups of fibers are affected. It may happen that the fibers are partially affected. If their ends are destroyed at the suture, then the cataract takes the shape of the suture. If a bigger part of the fiber is opaque, then the cataract has a shape of a flower. The fiber defect may not extend through the whole fiber and may shut down the healthy part of the fiber by an annealing process [29].

The appearance of vacuoles filled with fluid is seen under the capsule or the interior of the lens. They remain stationary for a long time, but with the age they eventually spread and in early cataracts large number of them appear under the capsule.

The three major cataract types are cortical, nuclear and subcapsular cataracts.

The cortical cataract has a shape of a wedge and it is located on the anterior or posterior cortex of the lens. It starts with a separation of the lamellae into series of fine parallel lines. The fibers are swollen and/or irregular, and there is a fluid filling the space between them [66]. The nuclei of the fibers close to the surface degenerate and disappear, and granularities appear in the cytoplasm. There is a decrease in the plasma density and vesiculation [67, 68, 69]. The ion exchange in the fibers is altered, which leads to osmotic imbalance in the cells [66].

Nuclear cataracts are the most common among the age-related cataracts. They do not have disordered or misplaced fibers, but there is an increase in the refractive index and density. These changes are due to the formation of protein aggregates, which scatter the light. The presence of the aggregates increases the optical density of the nuclei and later the fetal nucleus and the whole adult nucleus.

Subcapsular cataracts also have swollen fibers [70], but in addition the epithelial cells migrate towards the posterior pole and induce production of extracellular granular and fibrillary material [71]. Another author [66] describes the formation of a posterior subcapsular cataract as follows. Epithelial cells start migrating towards the posterior pole of the lens. Around the pole they form a cluster with a shape of a ring and

"form rounded-up balloon cells", which central part is liquid. The cells then produce a new basement membrane. "The balloon of bladder cells that cluster in a ring or circle around the center of the posterior pole interdigitate with the adjacent lens fibers, while the deeper cortical lens fibers are broken down into globules.

There are some chemical and conformation changes in the eye lens proteins which lead to cataract formation. These processes go slowly, and the cataract may appear years after it has been initiated. Normally there is increased scattering, absorption and fluorescence of the eye lens. The increase of light scattering is correlated to drastic changes of the density of the eye lens proteins and therefore the refractive index.

The metabolic changes in the eye lens are associated with increased amounts of sodium, calcium, lead, cadmium, hydrogen peroxide, malondialdehyde, nervonic acid, sugar phosphate (in diabetic cataracts), fluorophores and decreased amounts of glutathione,inositol, ascorbate and tetrahydropterin [21]. The ionic imbalance accompanies sixty seven per cent of the cataracts, most of which had nuclear and cortical changes. The increase in calcium level correleates with an increase of sodium. The diffusion coefficient is characteristic not only for the size of the aggregates, but its temporary changes can give information on the glucose levels in blood and aqueous humor [22].

There is a relatively high amount of bound water (it is bound to the surface of the protein molecules) in the eye lens due to the high protein concentration. Bound water has a lower freezing point than bulk water. If the protein structure is changed by posttranslational modifications or conformational changes [72, 73], then less water

would bind to them. The process by which the water is lost from the protein molecules is called syneresis. It was found to occur in both cortex and nucleus [74].

Another process characteristic for the cataracts is the increase of the insoluble proteins, again a consequence of the structural change of the proteins. Gamma - crystalline is covalently modified during cataract [75]. This is proved by the observation that the 10,000 Da polypeptide fractions that increase during the cataract formation are derived from gamma [76].

All the processes normal for the aging lens are found in the cataract formation. The difference is that in the latter they progress further.

Chapter 4

Particle Size Evaluation

4.1 Introduction

Information on the size of small particles has been of interest in biophysics, chemistry, astronomy, meteorology, remote sensing, environment monitoring and combustion [77, 78, 79, 80, 81, 82]. The most powerful techniques are optical because they are non-invasive, accurate and fast [83].

The theory of light scattering and absorption by small particles has been described in details in literature [84, 85, 86, 87], and only a summary of its features relevant to this work will be presented.

4.2 Scattering Techniques

The two major scattering techniques are static and dynamic light scattering. The Dynamic Light Scattering (DLS) method has been used for sizing of soot particles [88, 89], early detection of uveitis, cholesterol levels, and cataracts [90, 91]. It is considered to be very good for characterization of particle sizes in the Rayleigh regime (size parameter[1] x$\ll$1)[92, 93, 94, 95]. The DLS technique[2] is based on measurements of the autocorrelation function and the diffusion coefficient of the moving particles. The size of the assumed spherical particles is determined by the use of the Einstein relation:

$$D = \mu k_B T, \tag{4.1}$$

where T is the temperature, D is the diffusion coefficient, k_B is the Boltzmann's constant and μ is the mobility of the particle:

$$\mu = \frac{1 + A\frac{\lambda_m}{R_p} + Q\frac{\lambda_m}{R_p} exp(-b\frac{R_p}{\lambda_m})}{6\pi\eta R_p}, \tag{4.2}$$

where λ_m is the mean-free path of molecules in the surrounding gas, η is the dynamic viscosity of the ambient gas and R_P is the radius of the particle.The constants A, b and Q are well known[3]. The correlation function in case of a monodisperse particle size

[1] size parameter is defined as $x = \frac{2\pi d}{\lambda}$, where d is the radius of the particle and λ is the wavelength

[2] Also called Laser Doppler Spectroscopy (LDS), Diffusion Broadening Spectroscopy (DBS) and Light-Beating Spectroscopy

[3] A=0.86, Q=0.29, b=1.25

distribution function is given by [89]:

$$G(\tau) =< n_{\Delta\tau} >^2 [1 + exp(-2q^2 D\tau)], \tag{4.3}$$

where $< n_{\Delta\tau} >$ is the average number of photons per sampling interval, $q = \frac{4\pi n}{\lambda} sin(\frac{\vartheta}{2})$ is the scattering vector, n is the index of refraction of the surrounding medium, λ is the wavelength of the incident light in vacuum, τ is the time interval.

In case of a polydisperse PSDF the correlation function is proportional to [89]:

$$exp\{-[(\frac{t}{\tau_t})^2 + 2q^2 Dt]\}. \tag{4.4}$$

The advantages of this method are that there is no need for the refractive indices to be known and in addition to particle sizes, particle velocities can be determined.

Static Light Scattering Technique (SLS)[1] is suitable for polydisperse particle size distributions yield good results for a reasonably broad PSDF. The disadvantage of this method is that the data reduction can be very difficult [83]. In order to apply Mie theory for scattering/transmission experiments Petrovich, and then Sun [89, 83] assumed: particles are spheres randomly distributed in space and single scattering. The scattering cross-section is:

$$C_s(r, m, \theta_0, \Phi_0, \lambda) = \frac{1}{k^2} \int_{\Delta\Omega} d\Omega(|S_1|^2 sin^2\Phi + |S_2|^2 cos^2\Phi), \tag{4.5}$$

[1]extinction can beconsidered to be scattering with a zero scattering angle

where $\Delta\Omega$ is the solid angle subtended at the scattering center by the detector, S_1 and S_2 are the complex scattering matrix elements given by:

$$S_1 = \sum_{n=0}^{\infty} \frac{2n+1}{n(n+1)}(a_n\pi_n + b_n\tau_n) \tag{4.6}$$

$$S_2 = \sum_{n=0}^{\infty} \frac{2n+1}{n(n+1)}(a_n\tau_n + b_n\pi_n) \tag{4.7}$$

The PSDF, p(r), is then retrieved by solving the integral equation:

$$g(\alpha_i) = \int_0^{\infty} K(\alpha_i, r)p(r)dr, \tag{4.8}$$

where $i = 1, \ldots, n$; α_i represents the wavelength in the extinction case and the scattering angle in the scattering case and $K(\alpha_i, r)$ is the Mie Kernel function.

Yanji Tang [88] computed the scattering and extinction cross-sections of spheres and fractals, built with the same number of monomers and size parameter. His results show that "it is difficult to distinguish the structure configuration, or morphology, of the particles by static scattering technique for small size parameters (x<0.2)". Therefore the assumption of spherical shape of the particles does not significantly affect the result.

4.3 Multi-Wavelength Extinction Measurements

Multi-wavelength extinction measurements were done by Petrovic [89] and by Sun [83] for spherical particles and later by Tang [88] for spherical particles and fractals.

The transmittance of a monochromatic beam obeys the Lambert-Beer Law:

$$\frac{I(\lambda)}{I_0(\lambda)} = exp(-\tau_t), \tag{4.9}$$

where τ_t is called the optical thickness and it can be written as:

$$\tau_t = NL \int_0^L \int_0^\infty C_e(\lambda, r, l, m) p(r) dr. \tag{4.10}$$

$C_e(\lambda, r, l, m)$ is the Mie extinction cross-section for each particle with radius r, m is the relative complex refractive index[1]

The particle size distribution function is assumed to be log-normal distribution, which appears to be natural for growth processes:

$$p(d) = \frac{1}{\sqrt{2\pi}d}\Big(-\frac{(logd - \mu)^2}{2\sigma^2}\Big). \tag{4.11}$$

The mean particle diameter D and the standard variance are given by:

$$D = exp\Big(\mu + \frac{\sigma^2}{2}\Big) \tag{4.12}$$

$$V^2 = exp(2\mu + \sigma^2)[exp(\sigma^2) - 1] \tag{4.13}$$

This function is capable of describing broad size distributions, as well as narrow size distributions [83]. The size distribution function is retrieved from the experimental data

[1] $m = \frac{n_p}{n_m}$, n_p is the refractive index of the particle and n_m is the refractive index of the media

by solving equation (4.8).

4.4 Downhill Simplex Method

The goal of the method is to find the extremum of a function by adjusting the parameters of the PSDF. As described by Sun:".. simplex is a geometrical figure formed (for a M dimensional problem) by M+1 points in a M dimensional coordinate system including all polygonal faces and lines connecting the points." The initial simplex is made of points which are the initial guess. The values of the function are evaluated in each point and the point with the highest value across the opposite face of the figure to reach a lower point. Then, depending on the functional values, it may be expanded or contracted in one or more directions. The procedure ends when the difference in the functional values in all points is very small. In the case the particle scattering or deconvolution, the function to be minimized is:

$$\chi^2 = (\vec{t} - \vec{g}_e)^2 = (\vec{t} - \vec{g} - \vec{\varepsilon}), \tag{4.14}$$

where $\vec{t}$ is the trial data vector;$\vec{g}$ is the true data and $\vec{\varepsilon}$ is the experimental error.

$$\vec{t} = K.\vec{f} \tag{4.15}$$

where $\vec{f}$ is the trial vector for the particle size distribution function [83]. The fit is considered to be good if $d^2 < \chi_{min} \leq \varepsilon^2$, where $d = |\vec{t} - \vec{g}|$. In this calculation the

trial vector $\vec{t}$ is changed by changing the trial distribution function f by adjusting μ and σ, and therefore the mean diameter and the variance. The number density and the complex index of refraction can also be varied for more complete information from the data.

4.5 Monte Carlo Simulations

Monte Carlo simulations were applied by Petrovic and then by Sun to deconvolve the PSDF of soot particles and water droplets. The deconvolution results show good agreement with the experimental data in both studies.

First a set of synthetic data $\vec{g}$ was generated. Then for each data value g_i a random error ε_i was added. The noisy data were used as experimental data, which were used to perform the deconvolutions and the result would be the mean diameter of the particles D, the variance of the distribution V, and/or the product NL. Steps 2 and 3 were repeated many times to obtain the statistical distribution of the parameters.

4.6 Cataract Size Evaluation

Most of the experiments done so far to determine the protein aggregates sizes are based on the DLS technique. In 1975, Tanaka and Benedek measured the mean diffusivity of normal and cataractous lenses *in vitro* for different temperatures and locations [23]. The results (see Fig.4.1 and Fig.4.2) show that at the same temperature, the diffusivity, and therefore the size of the proteins differ considerably in a normal and cataractous

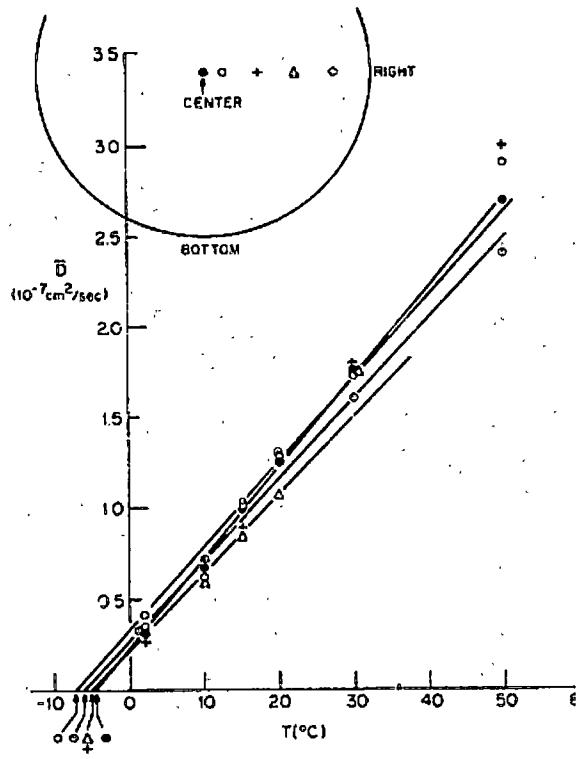


Figure 4.1: Mean diffusivity in a normal human lens as a function of temperature and position in the lenses [23].

lenses. In the cataractous lens they examined there was no spatial variation in the size distribution or the protein concentration. The diffusivity is much smaller than in a normal lens which shows the occurrence of large protein aggregates. The curvature of the plot also shows that the nature of the protein interactions are different in case of such a lens in comparison of the interactions in a normal lens. As an example, let us take the mean diffusivity of a normal lens (in the central part) at $36°C$, $2 \times 10^{-7} cm^2/s$ and the diffusivity of a cataractous lens at the same temperature, $0.35 \times 10^{-7} cm^2/s$. If we assume the dynamic viscosity is 0.6915 centipoise, as given by Ansari [96], then by using

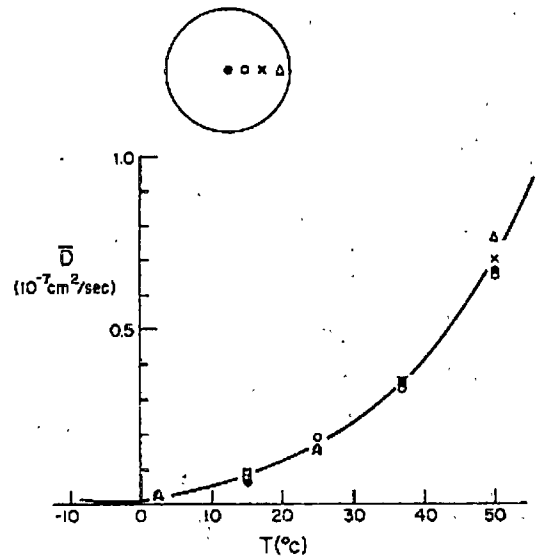


Figure 4.2: Mean diffusivity in cataractous human lenses as a function of temperature and position.

the Einstein relation 4.1, we obtain protein sizes of 16.36nm and 93.5nm, respectively.

In 1981 Siew and Bettelheim [91] used a SLS technique to estimate the spatial and age-related changes in the size of the proteins in a normal human lens. The results are given on Fig.4.3. Fig.4.3 shows the differences in the protein sizes at different ages at different locations in the lens (the numbers accompanying the lines on the graph represent the distance from the center of the lens). The conclusion is that while the size of the aggregates increases in the cortex with age, it tends to decrease in the nucleus. The other observation is that the volume fraction of the aggregates (Fig.4.4) decreases with age more steeply in the center. This seems to be in a contradiction with other authors, who found out that the molecular weight of the proteins in the center of the lens and their concentration are greater that in the cortex. The authors argue that the molecular weight should be distinguished from the size, as well as concentration in

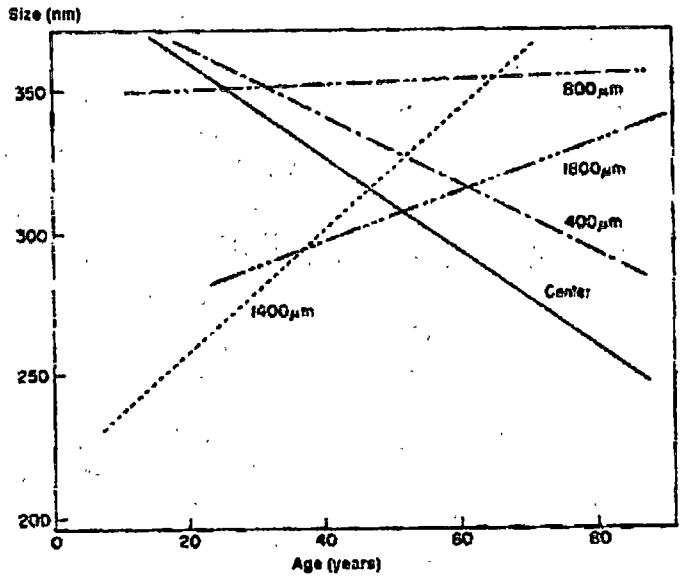


Figure 4.3: Size of the protein aggregates as a function of age.

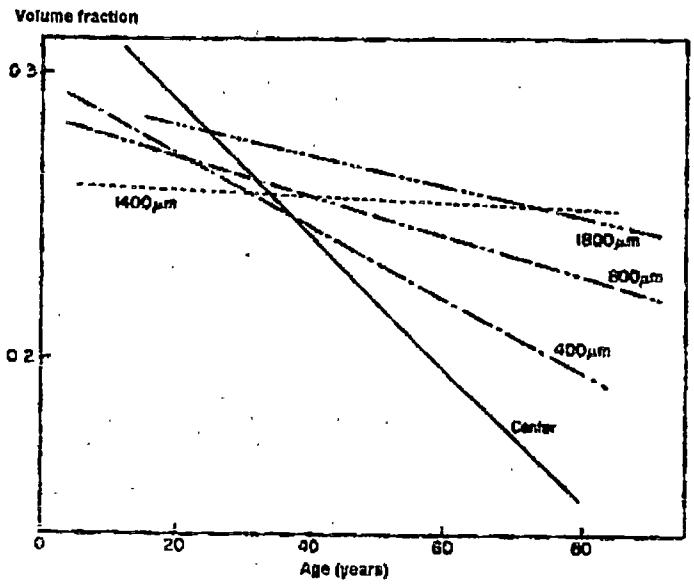


Figure 4.4: Volume fraction of the protein aggregates as a function of age.

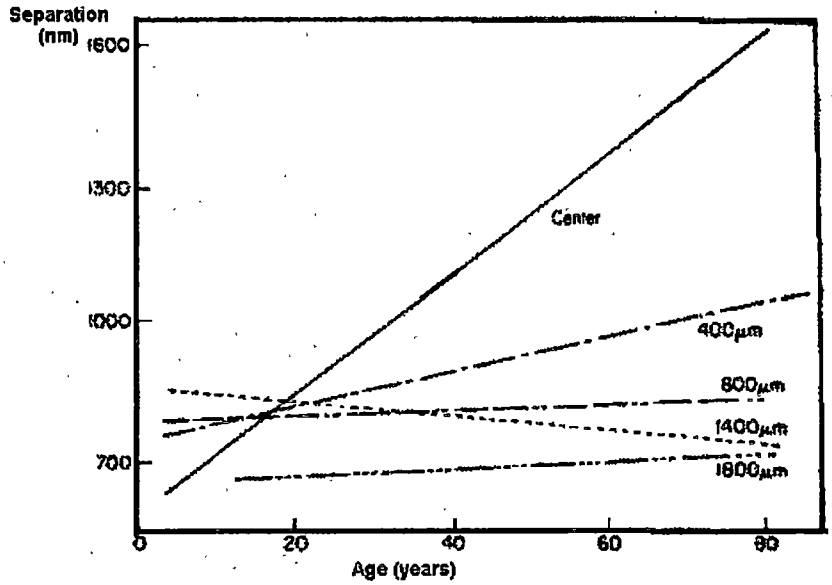


Figure 4.5: The average distance of separation of protein aggregates as a function of age.

terms of g/cm^2 versus volume fraction. They concluded that the protein aggregation is accompanied by a "strong collapse of the protein network". Therefore the aggregates are heavier, but smaller and denser.

In 1996 Karsten Dirks used the DLS method *in vivo* to determine the sizes of cataracts in normal and cataractous lenses. He also wanted to see if there was a correlation between the Scheimflug photographic density of pictures of lenses and his measurements. His results (Fig. 4.6,4.7,4.8) show that the small and the large components of the protein aggregates were 5.13 $\pm$ 1.6 nm and 690 $\pm$ 470 nm for healthy eye lenses, and 880 $\pm$ 460 nm for cataractous lenses. A good agreement with the Scheimflug technique is shown.

By applying the same technique, Ansari measured two sizes of protein aggregates, 41.14 $\pm$ 2.85 nm (whithin7 percent) and 3.08 $\pm$ 0.52 μm (whithin 17 percent) [96].

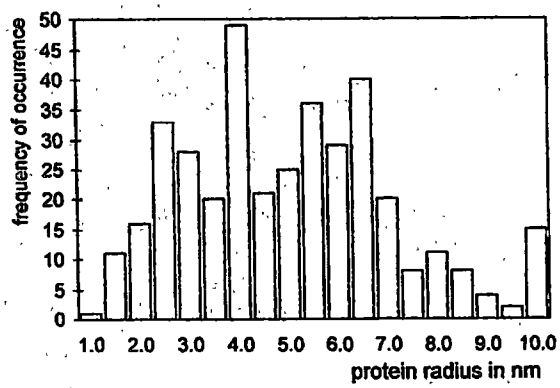


Figure 4.6: Histogram of the radius of the small proteins [24].

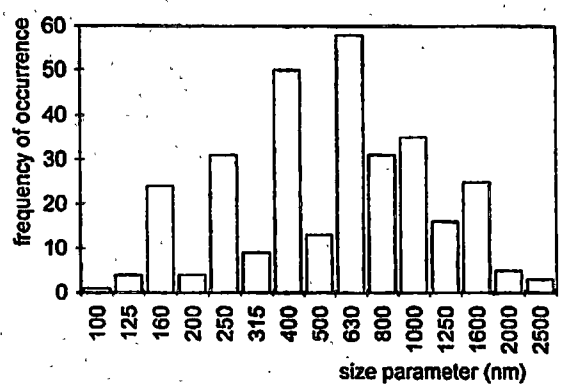


Figure 4.7: Histogram of the radius of the large proteins [24].

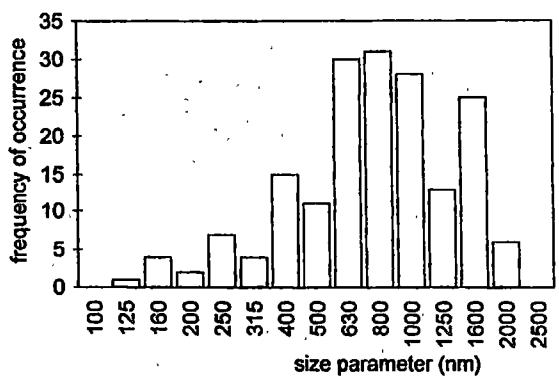


Figure 4.8: Histogram of the radius of the large proteins in a cataractous lens [24].

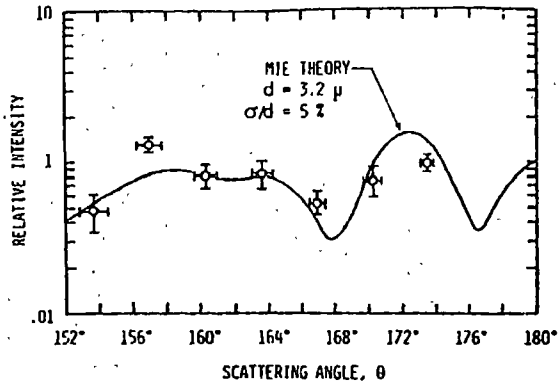


Figure 4.9: Relative scattering intensity from a rabbit cataract on the axis of the eye lens[25].

The normalized autocorrelation function is given as a function of the fluctuations of the scattered light amplitude $g^1(\tau)$ by:

$$g^2(\tau) = A[1 + \beta|g^1(\tau)|^2], \tag{4.16}$$

where $A =< i >^2$ is the average D. C. photocurrent, β is an experimentally determined constant and is a measure of the efficiency of the DLS spectrometer. $g^1(\tau)$ is given by the following form:

$$g^1(\tau) = I_\alpha exp(-D_\alpha q^2 \tau) + I_{\alpha A} exp(-D_{\alpha A} q^2 \tau) \tag{4.17}$$

In this equation I_α and $I_{\alpha A}$, D_α and $D_{\alpha A}$ are scattering strengths and the diffusion coefficients for the small and the large proteins, respectively; q is the scattering vector [90, 97, 96, 98].

Adam Bruckner applied an optical range-gating technique [25] and estimated (by applying Mie theory) the cataract size to be 3.2 μm on the eye lens axis and and 0.5 μm

2 mm off the eye lens axis (Fig.4.9) The relative index of refraction used in this paper was 1.09, which is the ratio of the protein refractive index of 1.45 and the refractive index of the surrounding media 1.33.

Chapter 5

Cataract Size Evaluation Using the Monte Carlo Method

5.1 Simulations

The particle size distribution function (PSDF) of cataracts was retrieved using the Monte Carlo method described in the previous section [81, 86, 87]. To simulate the signal from multiwavelength transmission measurements, the following "gedanken" experiment was designed. A light beam of diameter 1 mm with wavelengths in the ranges of 400 to 450 nm and 650 to 1000 nm illuminates the eye lens and the transmitted light is collected by a detector (see fig.). The relative index of refraction of the transmitting media was taken to have the same value as in Bruckner's experiment [25] 1.09. The transmission data (for a single pass through the eye lens) from this experiment was simulated using

the Lambert-Beer Law (eq.4.9). After that Gaussian distributed noise was added to the data, and the new data were used as experimental data to retrieve the PSDF[1]. Different particle size distribution functions were used to evaluate the sensitivity of the method. In the next section deconvolution results for two different distributions are shown. A two parameter (2-D) deconvolution is used if the mean diameter and the variance of the PSDF were to be obtained. The three-parameter (3-D) in addition to the mean diameter and variance parameters deconvolution gives the product NL, where N is the number density and L is the width of the slab (the eye lens in our case).

5.2 Small particles

The PSDF of small cataract particles is difficult to obtain because the relative refractive index is close to unity and the lack of absorption. Using only transmission data the PSDF parameters are hard to retrieve and the DHS method gets trapped in a local minimum. Despite that, the method showed potential to obtain the actual PSDF values. A PSDF with a mean diameter of 0.5 μm and a variance of 0.05μm was chosen to be representative for small cataracts. The deconvolution results are shown in the fig. 5.1 to 5.15. The histograms show the distribution of the deconvolved values (500 samples were taken) of the mean diameter, variance and the NL. The 2-D results give a good agreement for the mean diameter, but the variance is much larger then the assumed value. The 3-D deconvolutions show a better result. The mean value of the particle

[1]On the plots of the results the width of the Gaussian is given as sigma

diameter seems to be found for most of the error values, and the variance is still larger, but closer to the initial value. The NL are accurate for the most error levels.

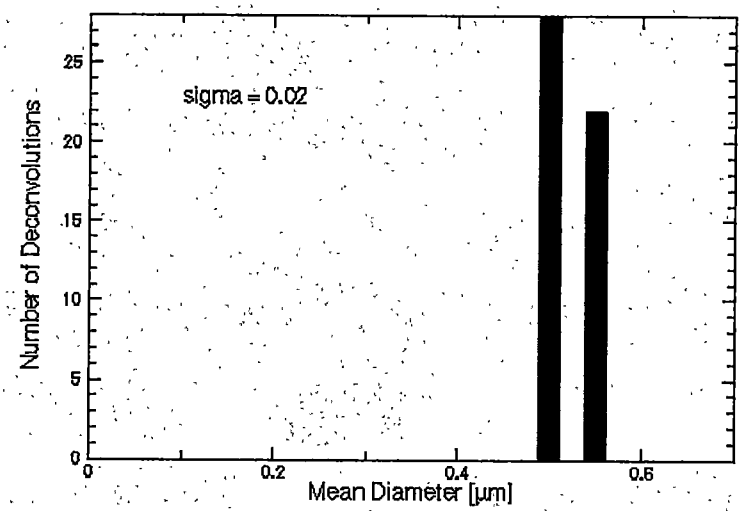


Figure 5.1: Histogram of the deconvolved particle diameters - 2D deconvolution. Assumed mean diameter 0.5 μm, error level 0.02.

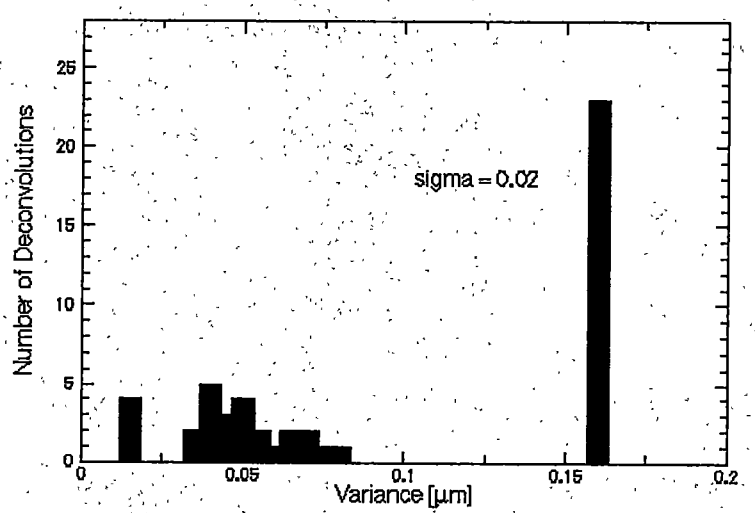


Figure 5.2: Histogram of the deconvolved variances - 2D deconvolution. Assumed variance 0.05 μm, error level 0.02.

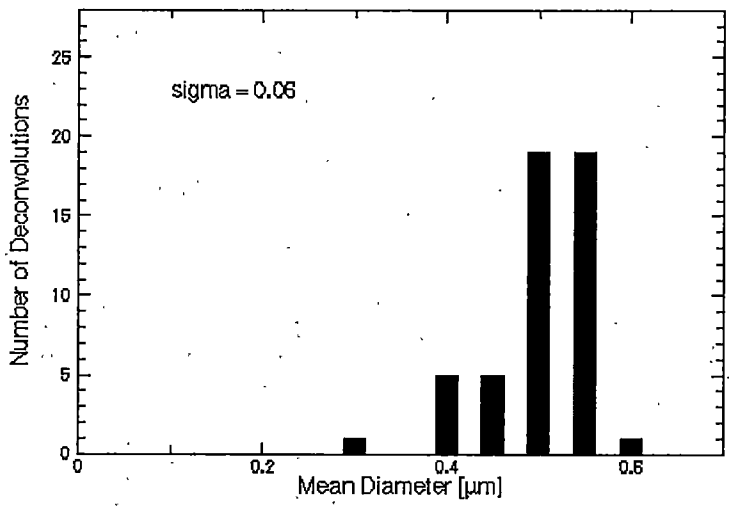


Figure 5.3: Histogram of the deconvolved particle diameters - 2D deconvolution. Assumed mean diameter 0.5 μm, error level 0.06.

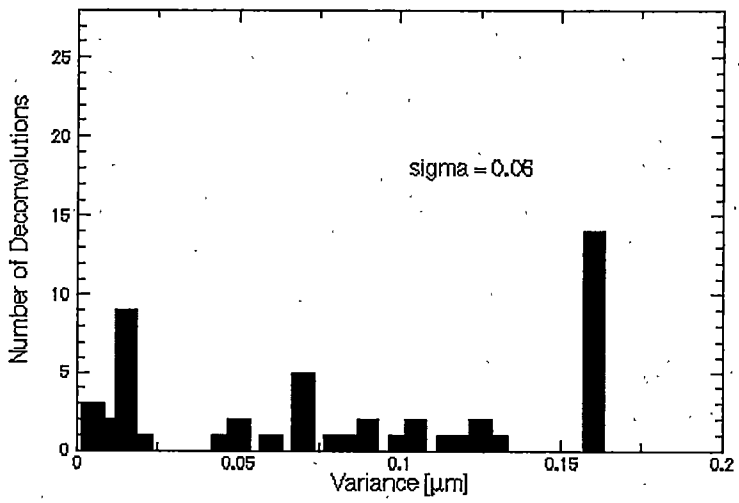


Figure 5.4: Histogram of the deconvolved variances - 2D deconvolution. Assumed variance 0.05 μm, error level 0.06.

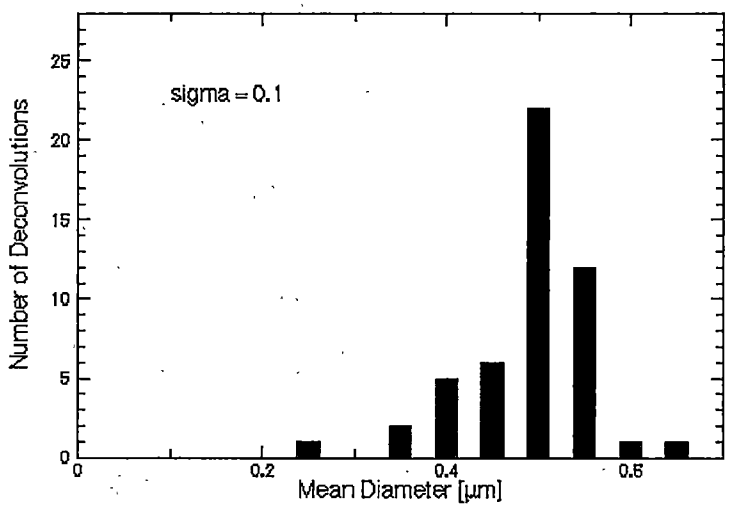


Figure 5.5: Histogram of the deconvolved particle diameters - 2D deconvolution. Assumed mean diameter 0.5 μm, error level 0.1.

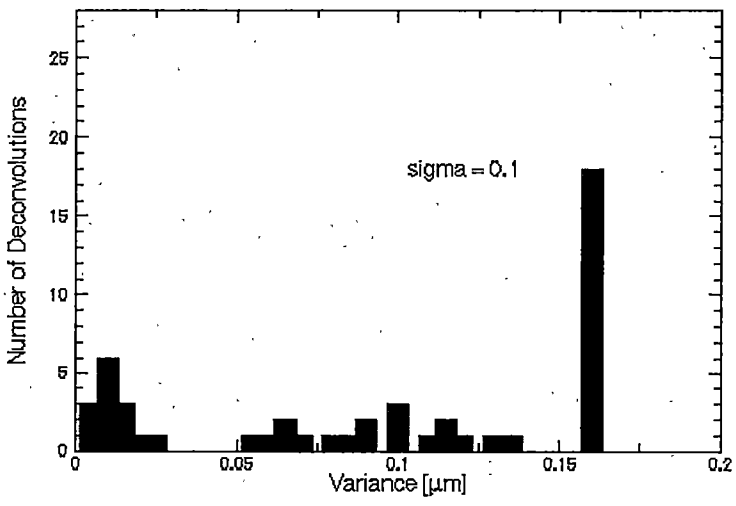


Figure 5.6: Histogram of the deconvolved variances - 2D deconvolution. Assumed variance 0.05 μm, error level 0.1.

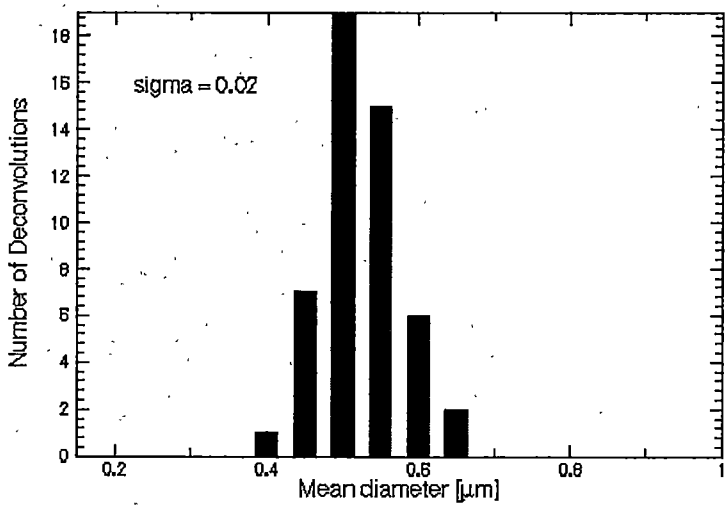


Figure 5.7: Histogram of the particle diameters - 3D deconvolution. Assumed mean diameter 0.5 μm, error level 0.02.

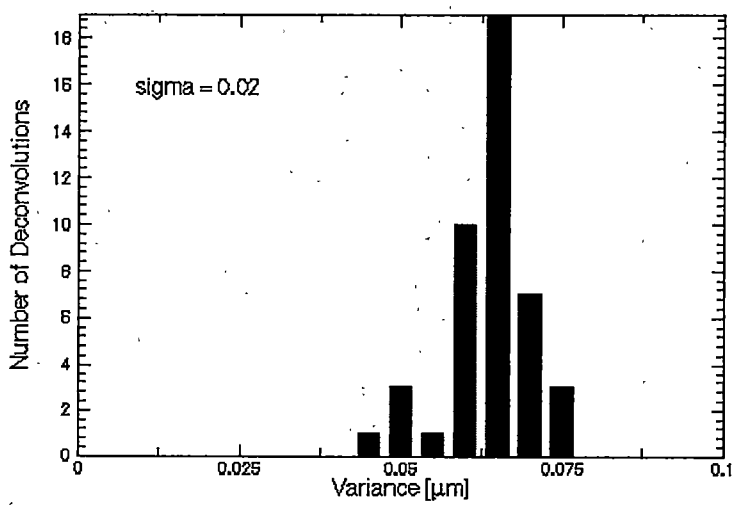


Figure 5.8: Histogram of the variances - 3D deconvolution. Assumed variance 0.05 μm, error level 0.02.

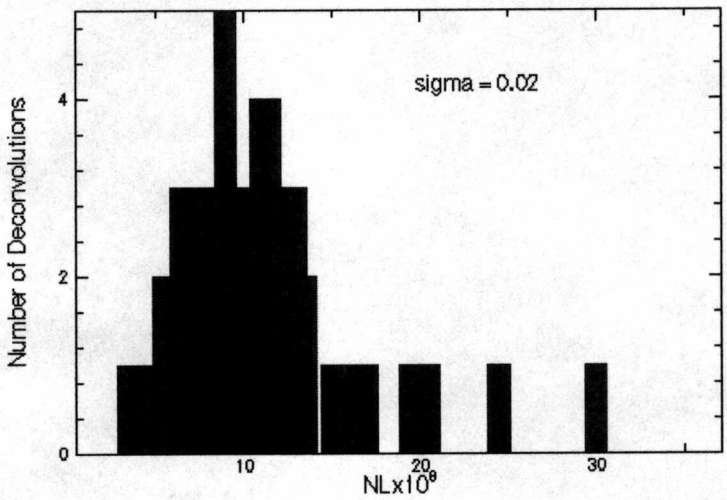


Figure 5.9: Histogram of the NL products - 3D deconvolution. Assumed $NL = 10^9 cm^{-2}$, error level = 0.02.

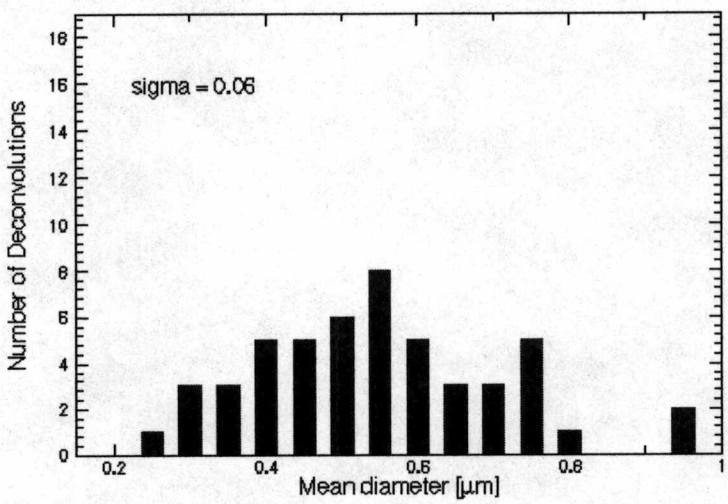


Figure 5.10: Histogram of the particle diameters - 3D deconvolution. Assumed mean diameter 0.5 μm, error level 0.06.

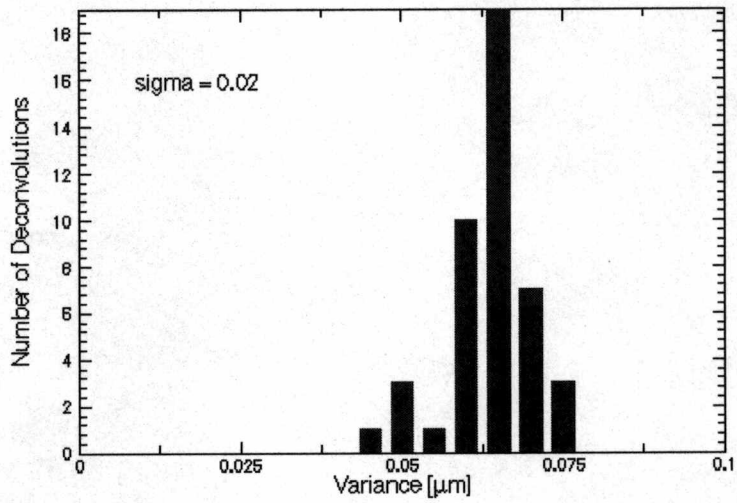


Figure 5.11: Histogram of the variances - 3D deconvolution. Assumed variance 0.05 μm, error level 0.06.

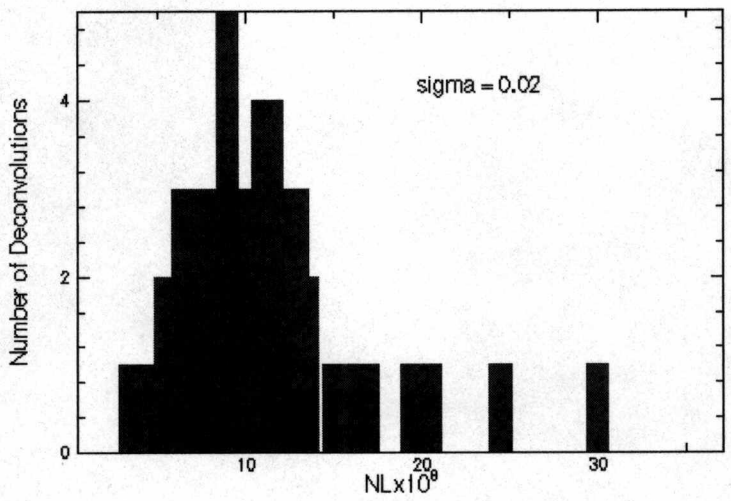


Figure 5.12: Histogram of the NL products - 3D deconvolution. Assumed $NL = 10^9 cm^{-2}$, error level = 0.06.

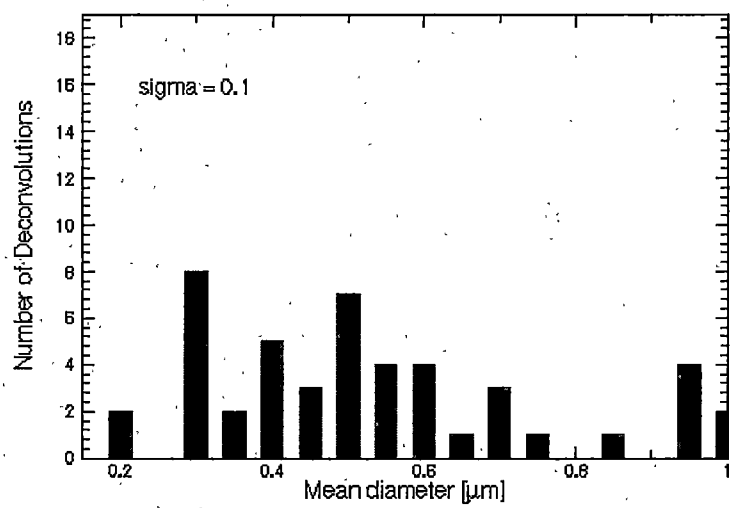


Figure 5.13: Histogram of the particle diameters - 3D deconvolution. Assumed mean diameter 0.5 μm, error level 0.1.

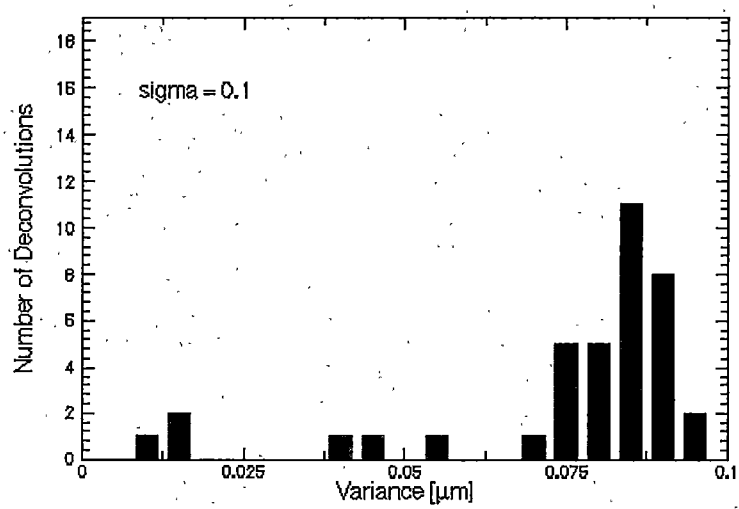


Figure 5.14: Histogram of the variances - 3D deconvolution. Assumed variance 0.05 μm, error level 0.1.

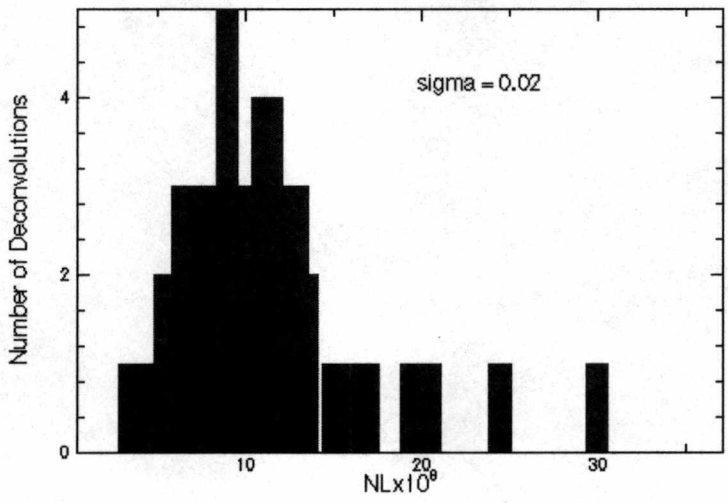


Figure 5.15: Histogram of the NL products - 3D deconvolution. Assumed $NL = 10^9 cm^{-2}$, error level = 0.1.

5.3 Large Particles

A mean size of 2.7 μm was chosen for the PSDF in case of large cataracts. The width of the distribution was chosen to be 0.135 μm. The results from this deconvolutions are shown in Fig.5.16 to Fig.5.26.

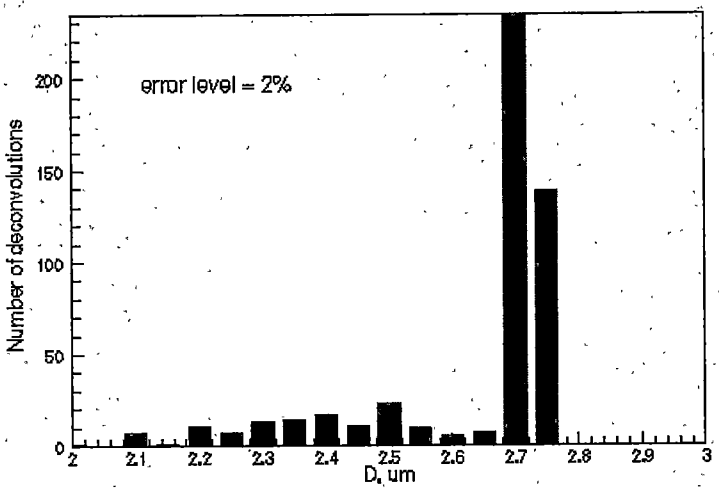


Figure 5.16: Histogram of the particle diameters - 2D deconvolution. Assumed mean diameter 2.7 μm, error level 0.02.

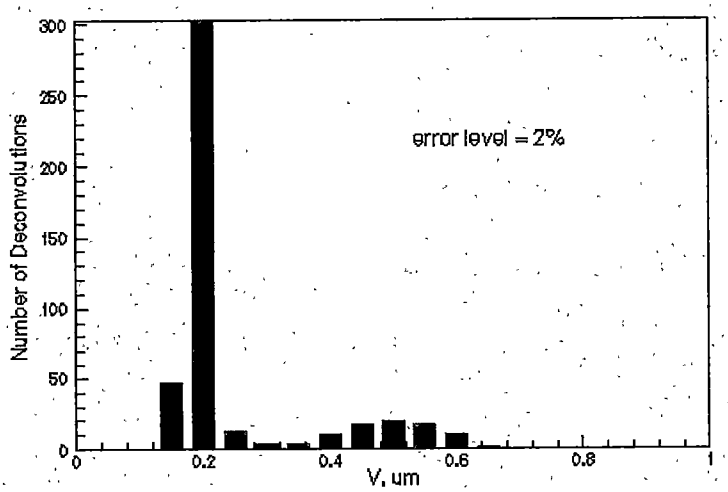


Figure 5.17: Histogram of the variances - 2D deconvolution. Assumed variance 0.135 μm, error level 0.02.

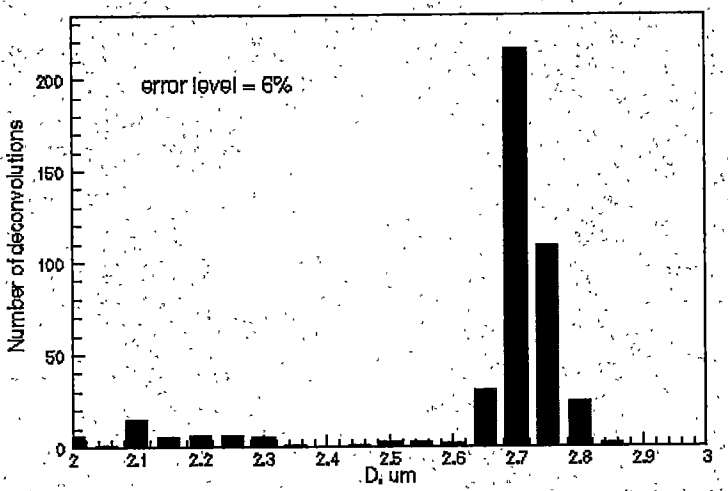


Figure 5.18: Histogram of the particle diameters - 2D deconvolution. Assumed mean diameter 2.7 μm, error level 0.06.

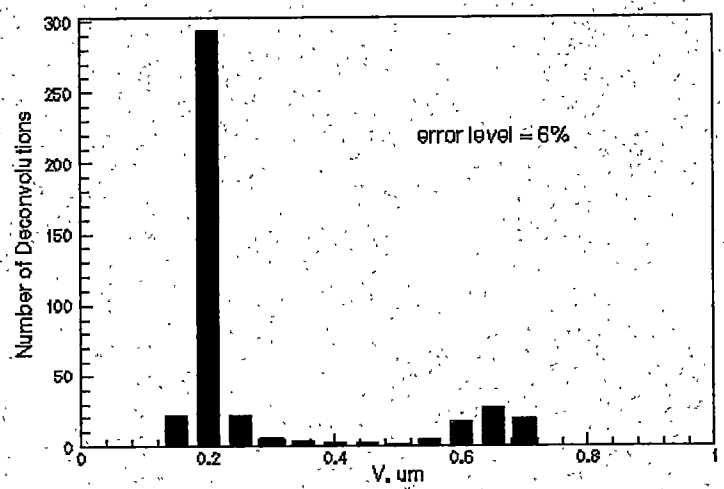


Figure 5.19: Histogram of the variances - 2D deconvolution. Assumed variance 0.135 μm, error level 0.06.

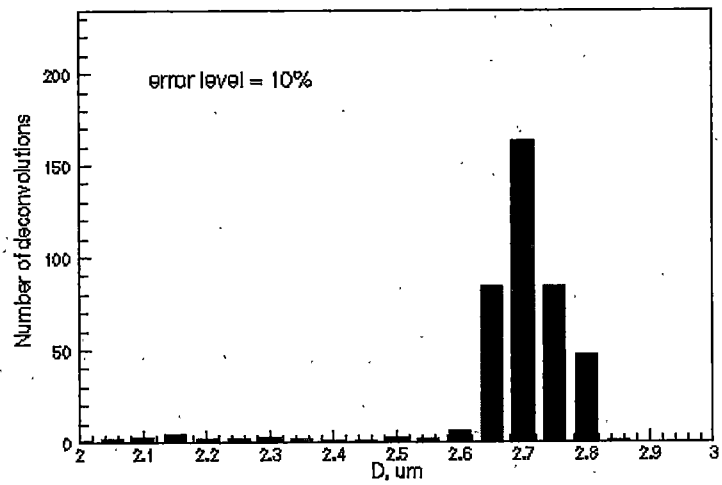


Figure 5.20: Histogram of the particle diameters - 2D deconvolution. Assumed mean diameter 2.7 μm, error level 0.1.

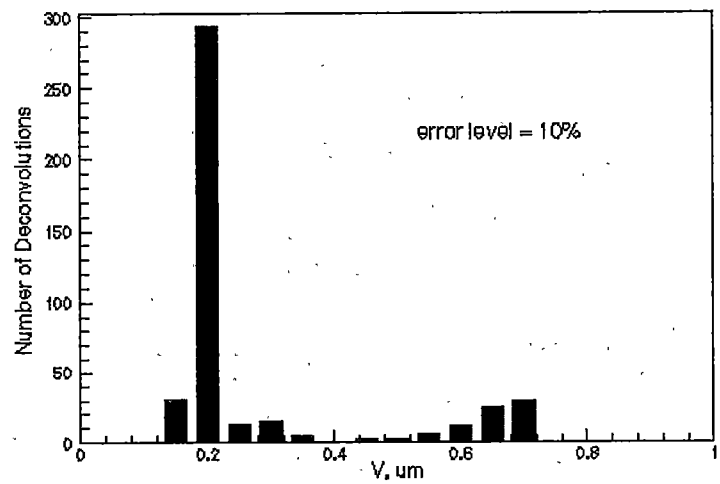


Figure 5.21: Histogram of the variances - 2D deconvolution. Assumed variance 0.135 μm, error level 0.1.

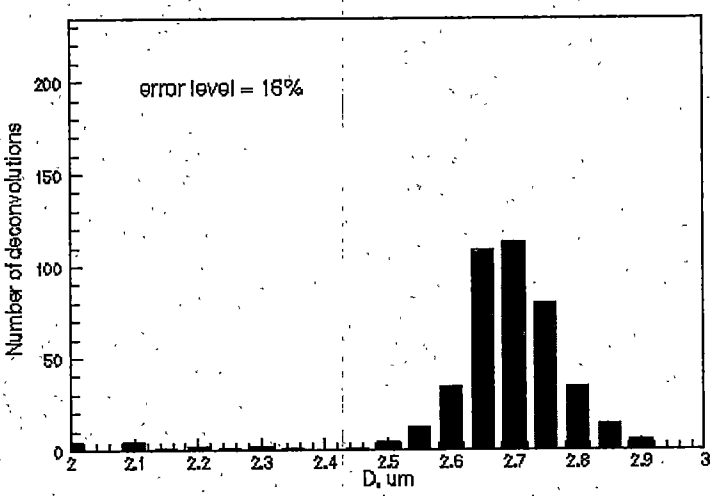


Figure 5.22: Histogram of the particle diameters - 2D deconvolution. Assumed mean diameter 2.7 μm, error level 0.16.

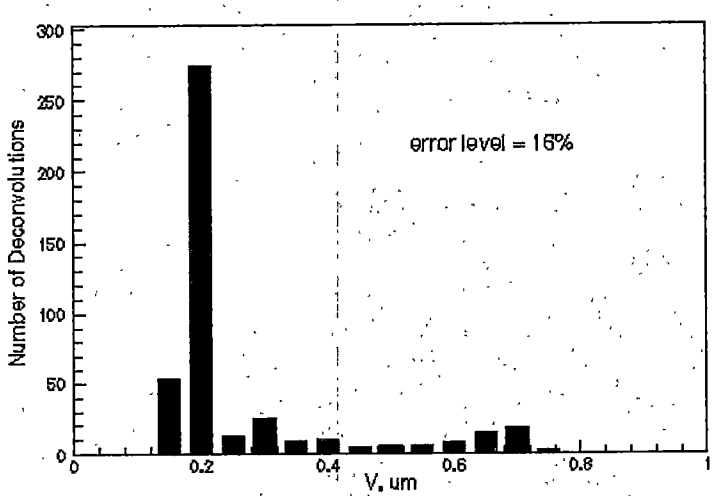


Figure 5.23: Histogram of the variances - 2D deconvolution. Assumed variance 0.135 μm, error level 0.16.

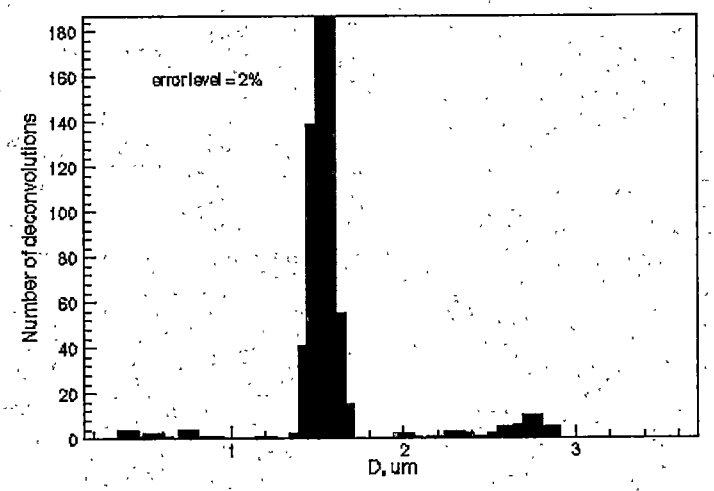


Figure 5.24: Histogram of the diameters - 3D deconvolution. Assumed mean diameter 2.7 μm, error level 0.02.

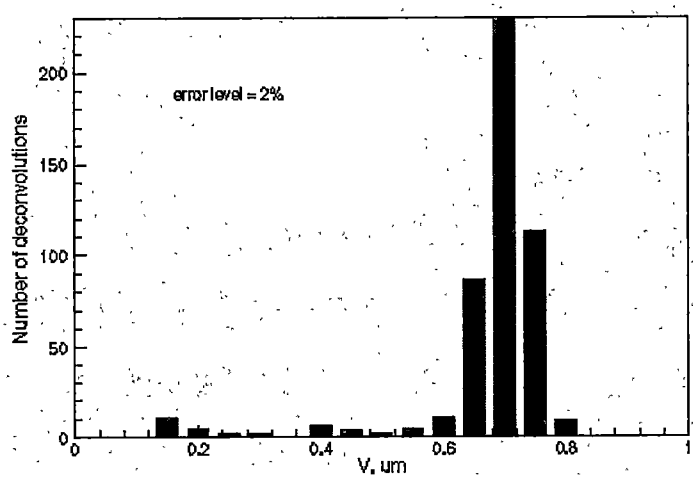


Figure 5.25: Histogram of the particle variances - 3D deconvolution. Assumed variance 0.135 μm, error level 0.02.

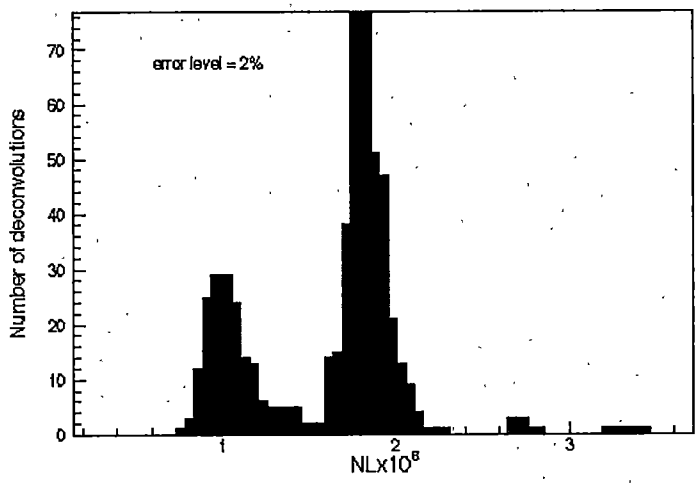


Figure 5.26: Histogram of the NL products - 3D deconvolution. Assumed $NL = 10^6 cm^{-2}$, error level = 0.02.

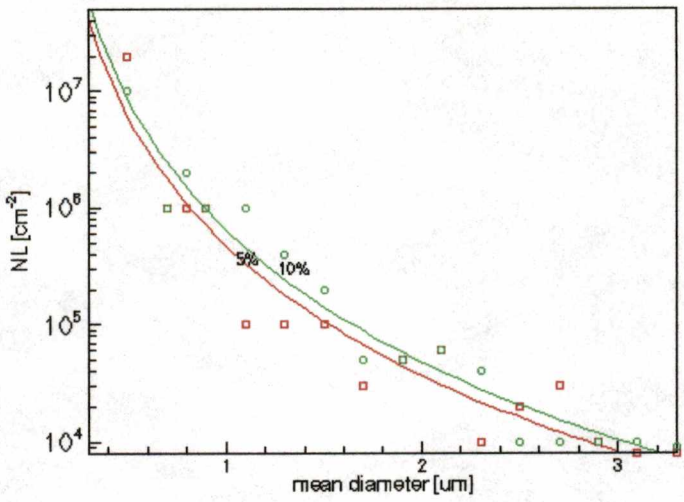


Figure 5.27: Minimum detectable NL for different particle sizes.

5.4 Sensitivity Calculations

Calculations were performed to evaluate the sensitivity of the Monte Carlo method, the following calculations were performed. First, transmission spectra for different particle diameters and different number densities (NL products, respectively) were simulated. On Fig.5.27 are given the minimum values of NL for which the calculation was successful[1]. Using this numbers the minimum detectable cataract volume was estimated.

The total observation volume is:

$$V_T = \frac{\pi d^2 L}{4} \tag{5.1}$$

where d is the beam diameter and L is the thickness of the central part of the eye lens.

[1]Successful means that the retrieved PSDF is close to the assumed one.

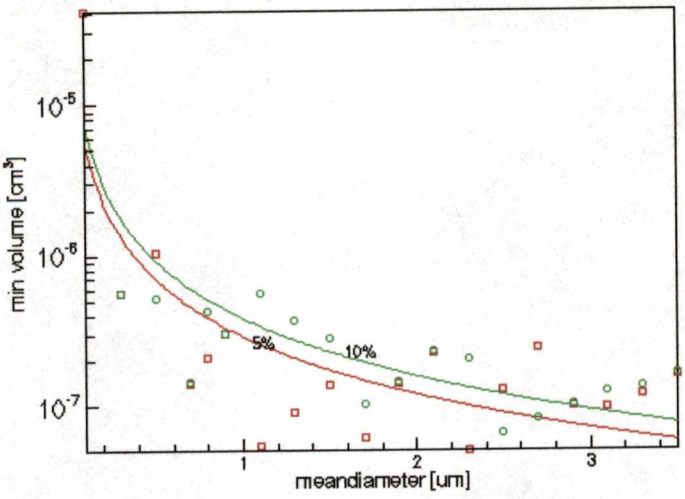


Figure 5.28: Minimum detectable volume for different particle sizes.

The total number of cataract particles is given by

$$n = N_T V_T \tag{5.2}$$

where N_T is the total number density of the cataract particles. The cataract volume is:

$$v_{cat} =< v > n \tag{5.3}$$

where $< v >$ is the mean volume of the distribution. The result for the minimum volume is presented on Fig.5.28.

Fig.5.29 shows that fraction of the observation volume that is occupied by the cataracts.

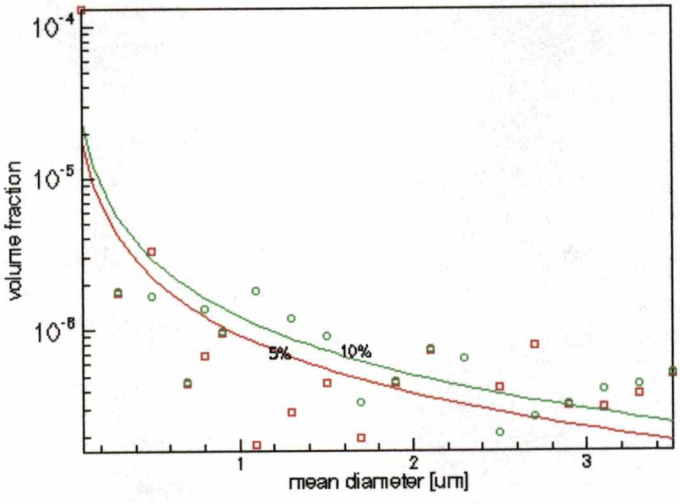


Figure 5.29: Minimum detectable fraction of the observation volume for different particle sizes.

5.5 Benchmark Calculations

The time for running the deconvolution program was estimated on a single machine, as well as a Condor loop of ten machines with the same processor speed. The distribution function used in all calculations had mean diameter of 2.7 μm and a variance of 0.132 μm.

The single PC calculation was carried on a machine with a 500 MHz processor speed. Each result Fig. 5.30 and Fig.5.31 represents the time for calculation for different numbers of deconvolutions and a different error levels added to the sythetic data. Each point on the plots represents the average time from ten runs for a particular number of deconvolutions and error level. In both the two-parameter and the three-parameter cases the higher the error level the more time it takes to calculate. The execution times are faster the lower the error level, but at the "sixteen per cent error" calculation shows a slightly decreased times. The time for a 100 deconvolutions increases from 384.5 s for 2 per cent error, 442.6 s for 25 per cent error to 595.3 s for 50 per cent error. The result for the 3D calculation followed the same trend. One hundred deconvolutions took 739.2 s for 2 per cent error level, 566.2 s for 25 per cent error level and 755.6 s for 50 per cents error level.

Condor is a resource managing program that can manage large heterogeneous clusters of workstations. It finds available machines on the network and uses tham for the program execution. In this calculation the task was distributed in the following way. If 100 deconvolutions were needed, 10 deconvolutions were submitted on every machine.

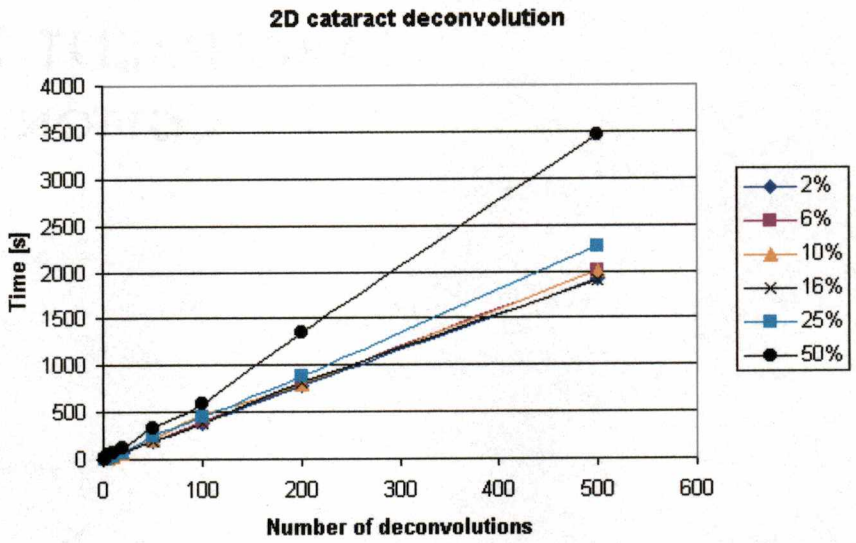


Figure 5.30: Benchmark for 2D deconvolution calculations on a single PC.

The results are given on Fig. 5.32 and 5.33. The time for the 2D calculation reduced to 209.62 s for 100 deconvolutions at 2 per cent error level and 225.6 s at 25 per cents error level. The 3D calculation for 100 deconvolutions took 190.3 s for 2 per cent error and 157.9 for 25 per cent error.

As a whole Condor is faster than a single PC as expected. However, there are some difficulties to perform deconvolutions for error levels larger than 25 per cent. This means that the program needs to be modified further in order to run better.

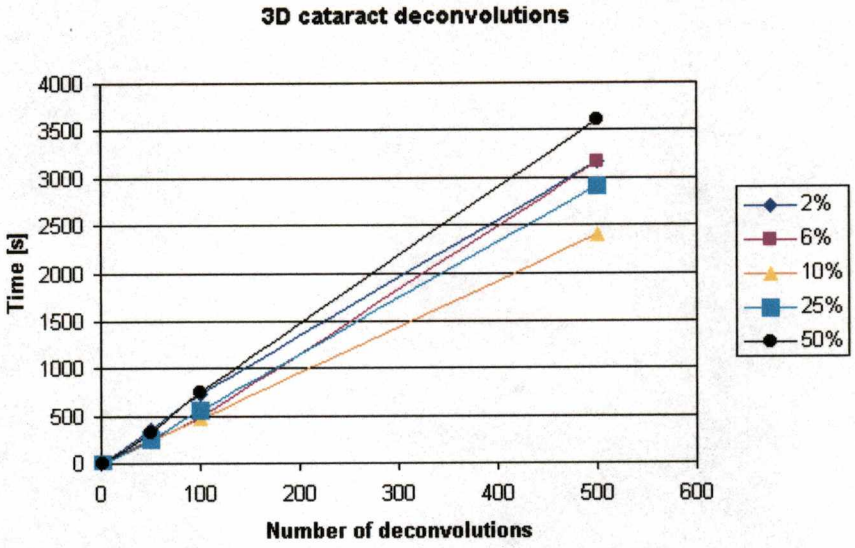


Figure 5.31: Benchmark for 2D deconvolution calculations on a single PC.

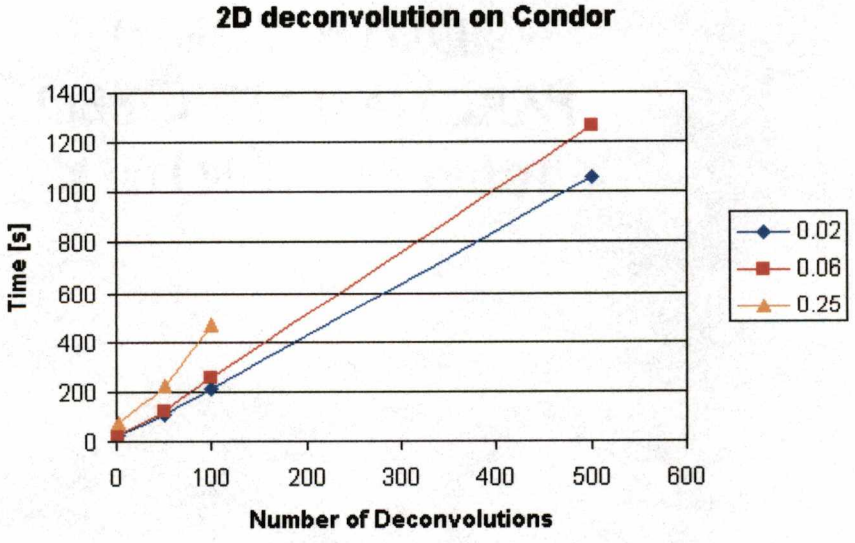


Figure 5.32: Benchmark for 2D deconvolution calculations on a Condor loop.

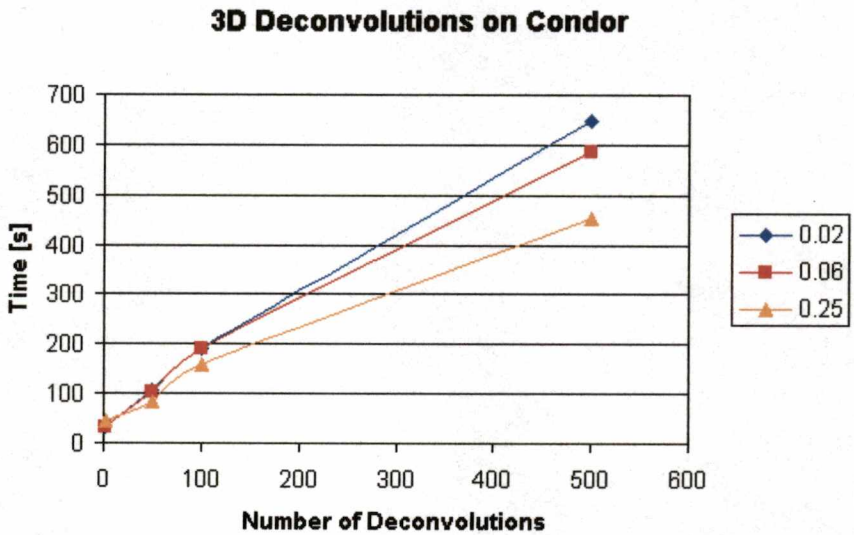


Figure 5.33: Benchmark for 2D deconvolution calculations on a Condor loop.

Bibliography

Bibliography

[1] K. Wright et al. *Textbook of Opthalmology.* Williams and Wilkins, 1997.

[2] J. F. Van Nostrand R. A. Cohen. Trends in the health of older americans: United states. *Vital Health Statistics*, 3(30), 1995. National Center for Health Statistics.

[3] J. G. Collins. Prevalence of selected chronic conditions: United states, 1990-1992. *Vital Health Statistics*, 10(194), 1997. National Center for Health Statistics.

[4] V. Benson and M.A. Marano. Current estimates from the national health interview survey, 1993. *Vital Health Statistics*, 10(190), 1995. National Center for Health Statistics.

[5] P. F. Adams and M.A. Marano. Current estimates from the national health interview survey, 1994. *Vital Health Statistics*, 10(193), 1995. National Center for Health Statistics.

[6] V. Benson and M.A. Marano. Current estimates from the national health interview survey, 1995. *Vital Health Statistics*, 10(199), 1998. National Center for Health Statistics.

[7] G. E. Hendershot P. F. Adams and M.A. Marano. Current estimates from the national health interview survey, 1996. *Vital Health Statistics*, 10(200), 1995. National Center for Health Statistics.

[8] National Advisory Eye Concil. Vision research, a national plan: 1999-2003, 1999.

[9] K. Sasaki et al. A new grading system for nuclear cataracts-an alternative to the japanese cooperative cataract epidemiology study group's grading system. *Developments in Ophthalmology*, 27:42–49, 1997.

[10] J. Horowitz N. S. Jaffe. *Optics and Refraction*, volume 1 of *Textbook of Opthalmology*. Gower Medical Publishing, 1992.

[11] LLC Light Lab Imaging. Oct.

[12] H. M. Merklinger. Scheimflug's patent. *Photo Techniques*, Nov/Dec 1996.

[13] European Molecular Biology Laboratory. http://www.embl-heidelberg.de.

[14] Protein Data Bank. http://www.rcsb.org/pdb/index.html.

[15] J. R. Wolter E. A. Boettner. Transmission of the ocular media. *Invest Ophthalmol*, 1:776–783, 1962.

[16] J. Pokorni. Aging of the human lens. *Applied Optics*, 26(8):1437–1440, 1987.

[17] R. Hemenger. Optical density of the crystalline lens. *American Journal of Optometry and Physiological Optics*, 59(1):34–42, 1982.

[18] E. F. McCarthy E. Ludvigh. Absorption of the light by the refractive media of the human eye. *Arch. Ophthalmol.*, 20:37–51, 1938.

[19] R. A. Weale. Light absorption by the lens of the human eye. *Opt. Acta (Lond)*, 1:107–10, 1954.

[20] B. K. Pierscionek. Variations in refractive index and absorbance of 670-nm light with age and cataract formation. *Experimental Eye Research*, 60:407–414, 1995.

[21] J. Horowitz N. S. Jaffe. *Lens and Cataract*, volume 3 of *Textbook of Opthalmology*. Gower Medical Publishing, 1992.

[22] J. Harding. *Cataract: biochemistry, epidemiology and pharmacology*. Chapman & Hall, 1991.

[23] T. Tanaka and G. B. Benedek. Observation of protein diffusivity in intact human and bovine lenses with application in cataract. *Investigative Ophthalmology*, 14(6):449–456, June 1975.

[24] K. Dierks et. al. Protein size resolution in human eye lens by dynamic light scattering after *in vivo* measurements. *Graefe's Arch. Clin. Exp. Ophthalmol.*, 236:18–23, 1998.

[25] A. P. Bruckner. Picosecond light scattering measurements of cataract microstructure. *Applied optics*, 17(19):3177–3183, October 1978.

[26] CDC. Cataract - a major blinding condition. *Morbidity and Mortality Weekly Report*, 32(9):119–20, March 1983.

[27] C. W. Taber. *Taber's cyclopedic medical dictionary.* F. A. Davis Company, 1997.

[28] E. R. Berman. *Biochemistry of the eye.* Plenum Press, 1991.

[29] N. P. Brown. *Lens Disorders: Clinical Manual of Cataract Diagnosis.* Butterworth-Heinemann Ltd, 1996.

[30] J. S. Hoffman. *Assessing the risks of trace gases that can modify the stratosphere*, volume 2. Environmental Protection Agency, 1987.

[31] J. Megaw S. Lerman and K. Gardner. Allopurinol therapy and human cataractogenesis. *Invest. Ophthal. Vis. Sci.*, 23:801–803, 1982b.

[32] L. Giacometty R. Hiller and K. Yuen. Sunlight and cataract: an epidemiological investigation. *Amer. J. Epidemiol.*, 105:450–459, 1977.

[33] M. Datiles S. Zigman and E. Torczinski. Sunlight and human cataracts. *Invest. Ophthal. Vis. Sci.*, 18:462–467, 1979.

[34] W. T. Jung et al. Racemidation of lens crystalline constituents in uv-induced cataract evaluated by chiral gc/ms spectroscopy. *Ophthalmic Research*, 28(S2):26–31, August 1996.

[35] Y. B. Shui et al. A new steroid-induced cataract model in the rat: long term prednisolone applications with minimum of x-irradiation. *Opthalmic Research*, 28(S2):92–101, August 1996.

[36] D. B. Judd S. M. Newhall, D. Nickerson. Final report of the D.S.A. subcommitee on the spacing of the munsell colors. *J. Opt. Soc. Am.*, 33:385–418, 1943.

[37] J. M. Sparrow N. A. Brown, A. J. Bron. Methods for evaluation of lens changes. *Int Ophthalmol.*, 12(4):229–35, 1998.

[38] N. A. Brown et al. The objective assessment of cataract. *Eye*, 1(Pt 2):234–46, 1987. Review.

[39] N. A. Sparrow et al. Decimalization of the Oxford clinical cataract classification grading system. *Ophthalmic Epidemiology*, 7(1):49–60, March 2000.

[40] J. M. Sparrow et al. The Oxford clinical cataract classification and grading system. *Int Ophthalmol*, 9(4):207–25, December 1986.

[41] J. R. Thompson et al. Associations between lens features assessed in the Oxford cataract classification and grading system. *Ophthalmic Epidemiology*, 4(4):207–12, December 1997.

[42] The Age Related Eye Disease Study. The age-related eye disease study (AREDS) system for classifying cataracts from photographs: AREDS report no. 4. *American Journal of Ophthalmology*, 131(1):167–175, February 2001.

[43] L. T. Chylack et al. Classification of human senile cataractous change by the American cooperative cataract research group (CCRG) method. *Investigative Ophthalmology and Visual Sciense*, 24:424–431, 1983.

[44] A. B. Hall et al. LOCSIII versus Oxford clinical cataract classification grading system for the assessment of nuclear, cortical and subcapsular cataract. *Ophthalmic Physiol Opt.*, 15(1):49–52, January 1995.

[45] H. R. Taylor J. R. Lee. Evaluation of photographic methods for documentation of opacities. *Invest Ophthalmol Vis Sci.*, 31(6):1191–3, June 1990.

[46] J. P. Gilman. Photo slitlamp biomicrography. http://webeye.ophth.uiowa.edu/ops/op-photo/slitlamps/slitlamp.htm, 1996.

[47] B. R. Masters et al. Three dimensioanal volume visualization of the *in vivo* human ocular lens schowing localization of cataract. *Ophthalmic Research*, 28(S2):120–126, August 1996.

[48] C. D. DiCarlo et al. Comparison of optical coherence tomography imaging of cataracts with histopathology. *Journal of Biomedical Optics*, 4(4):450–458, October 1999.

[49] A. F. Fercher. Optical coherence tomography. *Journal of Biomedical optics*, 1(2):157–173, April 1995.

[50] J. G. Fujimoto S. R. Chinn, E. A. Swanson. Optical coherence tomography using a frequency-tunable optical source. *Optics Letters*, 22(5):340–342, March1 1997.

[51] Kazuo Hotate Zhyuan He. Synthesized optical coherence tomography for imaging scattering objects by use of a stepwise frequency-modulated tunable laser diode. *Optics Letters*, 24(21):1502–1504, November1 1999.

[52] B. R. Masters. Optical tomography of the *in vivo* human lens: Three dimensional visualisation of cataracts. *Journal of Biomedical Optics*, 1(3):289–295, July 1996.

[53] H.-J. Huebscher et al. Laser Scheimflug videography. *Ophthalmic Research*, 28(s2):127–130, August 1996.

[54] K. H. Shyn et al. Normal aging changes of the scattering light intensity in human lens measuring with Scheimflug photography. *Developments in Ophthalmology*, 27:14–18, 1997.

[55] H. Goldmann. Biomicroscopy of the eye. *American Journal of Ophthalmology*, 66(5):789–804, November 1968.

[56] P. Egner. Entwicklung eines electronischen Scheimflugsystems zur untersuchung von linsentruebungen. Master's thesis, Ludwig-Maximilians University Muenchen, 1998.

[57] M. Wolbarsht D. Sliney. *Safety with Lasers and Other Optical Sources*. Plenum Press, 1980.

[58] J. Horowitz et al. Lens α-crystallin: function and structure. *Eye*, 13:403–408, 1999.

[59] L. Takemoto D. L. Boyle. A possible role for α-crystallins in lens epitelial cell differentiation. *Molecular Vision*, 6:63–71, May 2000.

[60] P. Russel C. Chambers. Sequence of the human lens β-b2-crystallin-encoding cdna. *Gene*, 133(295-9), 1993.

[61] G. B. Benedek. Theory of transparency of the eye. *Applied Optics*, 10:459–73, 1971.

[62] R. A. Weale F. S. Said. The variation with age of the spectral transmissivity of the living human crystalline lens. *Gerontologia(Basel)*, 3:213–31, 1959.

[63] H.-Lan Liou and N. A. Brennan. Anatomically accurate, finite model eye for optical modeling. *J. Opt. Soc. Am. A*, 14(8):1684–1695, August 1997.

[64] Zhixiang Ma et al. Age-related changes in human lens chrystallins identified by hplc and mass spectrometry. *Exp. Eye. Res.*, 67:21–30, 1998.

[65] N. Akthar Tian-Xiao Sun and J. J. N. Liang. Conformational change of human lens insoluble α crystallin. *Journal of Protein Chemistry*, 17(7):679–684, 1998.

[66] J. F. Amos. *Diagnosis and management of vision care.* Butterworth-Heinemann, 1987.

[67] T. Kuwabara. Maturation of the lens cell: A morphological study. *Exp. Eye Res.*, 20, 1975.

[68] A. Brini and J. Flament. Cataracta glaucomtosa acuta. *Exp. Eye Res.*, 16:19–28, 1973.

[69] G. Vrensen and B. Willekens. Biomicroscopy and scanning electron microscopy of early opacities in the aging human lens. *Invest. Ophthalmol. Vis. Sci.*, 31:1582–1591, 1990.

[70] H. Matsuura M. Nagata and Y. Fujinaga. Ultrastructure of posterior subcapsular cataract in human lens. *Ophthalmic Res.*, 18:180–184, 1986.

[71] J. Eshagian and B. W. Streeten. Human posterior subcapsular cataract. an ultrastructural study of the posterior migrating cells. *Arch. Ophthalmol.*, 98:134–143, 1980.

[72] J. J. Harding. The origin of urea-insoluble protein isolated from rat lens. *Exp Eye Res*, 14(3):289–90, Nov 1972.

[73] A. V. Krivandin et. al. A structural study of crystallins in the normal and cataractous crystalline lens by x-ray diffraction. *Oftalmol Zh*, 6:365–6, 1989.

[74] O. White L. T. Chylack Jr F. A. Bettelheim, J. A. Castoro. Topographic correspondence between total and non-freezable water content and the appearance of cataract in human lenses. *Curr Eye Res*, 5(12):925–32, December 1986.

[75] J. S. Zigler J. Horwitz L. J. Takemoto, J. S. Hansen. Characterization of polypeptides from human nuclear cataracts by western blot analysis. *Exp Eye Res*, 40(2):205–12, February 1985.

[76] J. Horwitz L. Takemoto, B. Straatsma. Immunochemical characterization of the major low molecular weight polypeptide (10k) from human cataractous lenses. *Exp Eye Res*, 48(2):261–70, February 1989.

[77] S. G. Ackleson and R. W. Spinrad. Size and refractive index of individual marine particulate: a flow cytometric approach. *Appl. Opt.*, 27:1270–77, 1988.

[78] G. J. Streekstra et. al. Light scattering by blood cells in ekacytometry. *Appl. Opt.*, 32:2266, 1993.

[79] B. L. Lindner and R. G. Isaacs. Remote sensing of clouds by multi-spectrum sensors. *Appl. Opt.*, 32:2744, 1993.

[80] P. R. Shapiro. Interstellar polarization:magnetite dust. *Astrophysical Journal*, 201:151–64, 1975.

[81] M. D. Lechner and G. V. Schultz. On the wavelength dependence of light scattering of polymer solutions. *ibid*, 469.

[82] A. E. Green et al. Light scattering and size-altitude distribution of atmospheric aerosols. *ibid*, page 520.

[83] F. Sun. *Optical Measurement of Particle Size Distribution Function Using Downhill Simplex Method; Theory and Experiment.* PhD thesis, The University of Tennessee, Knoxville, Knoxville, TN, May 1994.

[84] P. W. Barber and S. C. Hill. *Light scattering by particles: computational methods.* World Scientific, 1990.

[85] M. Kerker. *The scattering of light and other electromagnetic radiation.* Academic, New York, 1969.

[86] K. S. Schmitz. *An Introduction to Dynamic Light scattering by Macromolecules.* Academic Press, Sam Diego, 1990.

[87] Van de Hulst. *Light scattering by small particles.* Dover, New York, 1957.

[88] Y. Tang. *Optical Determination of Size and Distribution for Small and Fractal Particles Using Static and Dynamic Light Scattering.* PhD thesis, The University of Tennessee Knoxville, October 1998.

[89] D. Petrovic. *Optical Determination of Hydrocarbon Particle Sizes Produced by Pyrolysis of Acetylene.* PhD thesis, The University of Tennessee Knoxville, May 1991.

[90] R. R. Ansari et. al. Monitoring austronaut health at the nanoscale cellular level through the eye. Technical Report NASA TM-2000-210041, NASA, 2000.

[91] D. Opalesky E. L. Siew and F. A. Bettelheim. Light scattering of normal human lens. ii. age dependence of the light scattering parameters. *Exp. Eye Res.*, 33:603–614, 1981.

[92] W. Hinds and P. Reist. Aerosol measurementby laser doppler spectroscopy - i. theory and experimental results for homodeneous aerosol. *Aerosol Science*, 3:501, 1972.

[93] W. Hinds and P. Reist. Aerosol measurementby laser doppler spectroscopy - ii. operational limits, effects of polydispersity, and applications. *Aerosol Science*, 3:515, 1972.

[94] B. J. Brene and R. Pekora. *Dynamic Light Scattering.* Wiley, 1976.

[95] N. Knable H. Z. Cummins and Y. Yeh. Observationof diffusion broadening of rayleigh scattered light. *Physical Review Letters*, 12:150, 1964.

[96] R. R. Ansari et. al. A new clinical instrument for the early detection of cataract using dynamic light scattering. Technical Report NASA/CR-2000-209955, NASA, 2000.

[97] R. R. Ansari et. al. A compact fiber optic eye diagnostic system. Technical Report NASA TM-107099, NASA, 1995.

[98] R. R. Ansari et. al. Ophthalmic diagnostics using a new dynamic light scattering fiber optic probe. Technical Report NASA technical memorandum 107049, NASA, 1995.

Vita

Pavlina Jetchkova Jeleva was born in November 26, 1974 in Shumen, Bulgaria. She graduated from the Mathematical High School in her hometown in 1991. During the first years in the University of Shumen she decided to continue her education specializing in the field of Biomedical Physics. In 1998 she became a fulltime student of the University of Tennessee Space Institute where she earned a Master of Science degree.